engineered tumor cells have been considered as candidates to enhance host immune responses.[28] Alternatively, immunomodulating antibodies such as anti-cytotoxic T-lymphocyte antigen 4 (CTLA-4) and anti-programmed cell death 1 (PD-1) have been considered to reactivate T cell function.[28,29] These approaches may also be effective to enhance the antitumor effect induced by RFA.

In conclusion, the results of this study show that RFA can enhance various TAA-specific T cell responses and the number of T cells induced is associated with HCC recurrence-free survival. To maintain the TAA-specific T cell responses induced by RFA and to improve the immunological effect for HCC, additional treatment by vaccine or immunomodulatory drugs might be useful.

References

1. Parkin DM, Bray F, Ferlay J, Pisani P. Global cancer statistics, 2002. CA Cancer J Clin 2005;55:74-108.
2. Davila JA, Morgan RO, Shaib Y, McGlynn KA, El-Serag HB. Hepatitis C infection and the increasing incidence of hepatocellular carcinoma: a population-based study. Gastroenterology 2004;127:1372-1380.
3. Lencioni R. Loco-regional treatment of hepatocellular carcinoma. HEPATOLOGY 2010;52:762-773.
4. Cho YK, Kim JK, Kim MY, Rhim H, Han JK. Systematic review of randomized trials for hepatocellular carcinoma treated with percutaneous ablation therapies. HEPATOLOGY 2009;49:453-459.
5. den Brok MH, Sutmuller RP, van der Voort R, Bennink EJ, Figdor CG, Ruers TJ, et al. In situ tumor ablation creates an antigen source for the generation of antitumor immunity. Cancer Res 2004;64:4024-4029.
6. Iida N, Nakamoto Y, Baba T, Nakagawa H, Mizukoshi E, Naito M, et al. Antitumor effect after radiofrequency ablation of murine hepatoma is augmented by an active variant of CC chemokine ligand 3/macrophage inflammatory protein-1alpha. Cancer Res 2010;70:6556-6565.
7. Araki T, Itai Y, Furui S, Tasaka A. Dynamic CT densitometry of hepatic tumors. AJR Am J Roentgenol 1980;135:1037-1043.
8. Japan LCSGo. Classification of Primary Liver Cancer. 2nd ed. [in English]. Tokyo, Japan: Kanehara & Co., Ltd.; 1997.
9. Desmet VJ, Gerber M, Hoofnagle JH, Manns M, Scheuer PJ. Classification of chronic hepatitis: diagnosis, grading and staging. HEPATOLOGY 1994;19:1513-1520.
10. Mizukoshi E, Nakamoto Y, Tsuji H, Yamashita T, Kaneko S. Identification of alpha-fetoprotein-derived peptides recognized by cytotoxic T lymphocytes in HLA-A24+ patients with hepatocellular carcinoma. Int J Cancer 2006;118:1194-1204.
11. Mizukoshi E, Nakamoto Y, Marukawa Y, Arai K, Yamashita T, Tsuji H, et al. Cytotoxic T cell responses to human telomerase reverse transcriptase in patients with hepatocellular carcinoma. HEPATOLOGY 2006;43:1284-1294.
12. Mizukoshi E, Honda M, Arai K, Yamashita T, Nakamoto Y, Kaneko S. Expression of multidrug resistance-associated protein 3 and cytotoxic T cell responses in patients with hepatocellular carcinoma. J Hepatol 2008;49:946-954.
13. Mizukoshi E, Nakamoto Y, Arai K, Yamashita T, Sakai A, Sakai Y, et al. Comparative analysis of various tumor-associated antigen-specific t-cell responses in patients with hepatocellular carcinoma. HEPATOLOGY 2011;53:1206-1216.
14. Ikeda-Moore Y, Tomiyama H, Miwa K, Oka S, Iwamoto A, Kaneko Y, et al. Identification and characterization of multiple HLA-A24-restricted HIV-1 CTL epitopes: strong epitopes are derived from V regions of HIV-1. J Immunol 1997;159:6242-6252.
15. Kuzushima K, Hayashi N, Kimura H, Tsurumi T. Efficient identification of HLA-A*2402-restricted cytomegalovirus-specific CD8(+) T-cell epitopes by a computer algorithm and an enzyme-linked immunospot assay. Blood 2001;98:1872-1881.
16. Sobin LH, Wittekind C. TNM Classification of Malignant Tumors. 6th ed. New York, NY: Wiley-Liss; 2002.
17. Sallusto F, Lenig D, Forster R, Lipp M, Lanzavecchia A. Two subsets of memory T lymphocytes with distinct homing potentials and effector functions. Nature 1999;401:708-712.
18. Butterfield LH, Meng WS, Koh A, Vollmer CM, Ribas A, Dissette VB, et al. T cell responses to HLA-A*0201-restricted peptides derived from human alpha fetoprotein. J Immunol 2001;166:5300-5308.
19. Komori H, Nakatsura T, Senju S, Yoshitake Y, Motomura Y, Ikuta Y, et al. Identification of HLA-A2- or HLA-A24-restricted CTL epitopes possibly useful for glypican-3-specific immunotherapy of hepatocellular carcinoma. Clin Cancer Res 2006;12:2689-2697.
20. Thimme R, Neagu M, Boettler T, Neumann-Haefelin C, Kersting N, Geissler M, et al. Comprehensive analysis of the alpha-fetoprotein-specific CD8+ T cell responses in patients with hepatocellular carcinoma. HEPATOLOGY 2008;48:1821-1833.
21. Kiuchi Y, Suzuki H, Hirohashi T, Tyson CA, Sugiyama Y. cDNA cloning and inducible expression of human multidrug resistance associated protein 3 (MRP3). FEBS Lett 1998;433:149-152.
22. Nakao M, Shichijo S, Imaizumi T, Inoue Y, Matsunaga K, Yamada A, et al. Identification of a gene coding for a new squamous cell carcinoma antigen recognized by the CTL. J Immunol 2000;164:2565-2574.
23. Frost M, Bobak JB, Gianani R, Kim N, Weinrich S, Spalding DC, et al. Localization of telomerase hTERT protein and hTR in benign mucosa, dysplasia, and squamous cell carcinoma of the cervix. Am J Clin Pathol 2000;114:726-734.
24. Yang D, Nakao M, Shichijo S, Sasatomi T, Takasu H, Matsumoto H, et al. Identification of a gene coding for a protein possessing shared tumor epitopes capable of inducing HLA-A24-restricted cytotoxic T lymphocytes in cancer patients. Cancer Res 1999;59:4056-4063.
25. Zea AH, Rodriguez PC, Atkins MB, Hernandez C, Signoretti S, Zabaleta J, et al. Arginase-producing myeloid suppressor cells in renal cell carcinoma patients: a mechanism of tumor evasion. Cancer Res 2005;65:3044-3048.
26. Hoechst B, Ormandy LA, Ballmaier M, Lehner F, Kruger C, Manns MP, et al. A new population of myeloid-derived suppressor cells in hepatocellular carcinoma patients induces CD4(+)CD25(+)Foxp3(+) T cells. Gastroenterology 2008;135:234-243.
27. Zerbini A, Pilli M, Penna A, Pelosi G, Schianchi C, Molinari A, et al. Radiofrequency thermal ablation of hepatocellular carcinoma liver nodules can activate and enhance tumor-specific T-cell responses. Cancer Res 2006;66:1139-1146.
28. Topalian SL, Weiner GJ, Pardoll DM. Cancer immunotherapy comes of age. J Clin Oncol 2011;29:4828-4836.
29. Sharma P, Wagner K, Wolchok JD, Allison JP. Novel cancer immunotherapy agents with survival benefit: recent successes and next steps. Nat Rev Cancer 2011;11:805-812.

Clinical Cancer Research

Association of *Interleukin-28B* Genotype and Hepatocellular Carcinoma Recurrence in Patients with Chronic Hepatitis C

Yuji Hodo[1], Masao Honda[1,3], Akihiro Tanaka[1], Yoshimoto Nomura[1], Kuniaki Arai[1], Taro Yamashita[1], Yoshio Sakai[1], Tatsuya Yamashita[1], Eishiro Mizukoshi[1], Akito Sakai[1], Motoko Sasaki[2], Yasuni Nakanuma[2], Mitsuhiko Moriyama[4], and Shuichi Kaneko[1]

Abstract

Purpose: Several single-nucleotide polymorphisms (SNP) in the interleukin-28B (*IL-28B*) locus have recently been shown to be associated with antiviral treatment efficacy for chronic hepatitis C (CHC). However, such an association with hepatocellular carcinoma (HCC) is unkno3 we investigated the association between the *IL-28B* genotype and the biology and clinical outcome of patients with HCC receiving curative treatment.

Experimental Design: Genotyping of 183 patients with HCC with CHC who were treated with hepatic resection or radiofrequency ablation (RFA) was carried out, and the results were analyzed to determine the association between the *IL-28B* genotype (rs8099917) and clinical outcome. Gene expression profiles of 20 patients with HCC and another series of 91 patients with CHC were analyzed using microarray analysis and gene set enrichment analysis. Histologic and immunohistochemical analyses were also conducted.

Results: The TT, TG, and GG proportions of the rs8099917 genotype were 67.8% (124 of 183), 30.6% (56 of 183), and 1.6% (3 of 183), respectively. Multivariate Cox proportional hazard analysis showed that the *IL-28B* TT genotype was significantly associated with HCC recurrence ($P = 0.007$; HR, 2.674; 95% confidence interval, 1.16–2.63). Microarray analysis showed high expression levels of IFN-stimulated genes in background liver samples and immune-related genes in tumor tissues of the *IL-28B* TG/GG genotype. Histologic findings showed that more lymphocytes infiltrated into tumor tissues in the TG/GG genotype.

Conclusions: The *IL-28B* genotype is associated with HCC recurrence, gene expression, and histologic findings in patients with CHC. *Clin Cancer Res; 19(7); 1827–37. ©2013 AACR.*

Introduction

Hepatocellular carcinoma (HCC) is the seventh most common cancer worldwide and the third most common cause of cancer mortality (1). HCC usually develops in patients suffering from chronic hepatitis B or chronic hepatitis C (CHC). Although hepatic resection has been considered the most efficient therapy for HCC, it is only suitable for 20% to 35% of patients because of poor hepatic reserve (2). Radiofrequency ablation (RFA) has therefore been introduced as a minimally invasive therapy for such cirrhotic patients and is widely applicable with little effect on hepatic reserve. Moreover, randomized (3, 4) and nonrandomized (5, 6) controlled studies revealed no statistical difference in patient survival between resection and RFA.

Despite these curative treatments of HCC, its recurrence remains common. Several studies have identified potential risk factors for HCC recurrence, including the presence of cirrhosis, high α-fetoprotein (AFP) levels, large tumor foci, and tumor multiplicity (7, 8).

The interleukin-28B (*IL-28B*) gene, also known as IFN-λ3, is a newly described member of the family of IFN-related cytokines (9) and shares the same biologic properties as type I IFNs (10). Recently, several single-nucleotide polymorphisms (SNP) in the *IL-28B* locus have been associated with the effectiveness of pegylated-IFN and ribavirin combination therapy for CHC (11, 12). We previously confirmed this relationship and revealed that the *IL-28B* genotype is associated with the expression of hepatic IFN-stimulated genes (ISG) in patients with CHC (13). Others have also described an association between the *IL-28B* genotype and the outcome of CHC therapy, biochemical factors, and histologic findings (14, 15); however, the relationship between the *IL-28B* genotype and the biology and clinical course of HCC remains unknown. In this study,

Authors' Affiliations: Departments of [1]Gastroenterology and [2]Human Pathology, Kanazawa University Graduate School of Medical Science; [3]Department of Advanced Medical Technology, Kanazawa University Graduate School of Health Medicine, Kanazawa, Ishikawa; and [4]Third Department of Internal Medicine, Nihon University School of Medicine, Tokyo, Japan

Note: Supplementary data for this article are available at Clinical Cancer Research Online (http://clincancerres.aacrjournals.org/).

Corresponding Author: Shuichi Kaneko, Department of Gastroenterology, Kanazawa University Graduate School of Medical Science, 13-1 Takara-Machi, Kanazawa, Ishikawa 920-8641, Japan. Phone: 81-76-265-2235; Fax: 81-76-234-4250; E-mail: skaneko@m-kanazawa.jp

doi: 10.1158/1078-0432.CCR-12-1641

Translational Relevance

Several single-nucleotide polymorphisms (SNP) in the interleukin-28B (*IL-28B*) locus have recently been shown to be associated with antiviral treatment efficacy in chronic hepatitis C (CHC). In this study, we investigated the association between the *IL-28B* genotype (rs8099917) and the biology and clinical outcome of patients with hepatocellular carcinoma (HCC) receiving curative treatment. Patients with the *IL-28B* TT genotype had a significantly higher incidence of HCC recurrence than patients with the TG/GG genotype. Gene expression profile and histologic analysis showed that the immune response and chronic hepatitis inflammation were more severe in patients with the TT genotype. Conversely, the expression of IFN-stimulated genes was upregulated and the immune response to tumors was more intense in those with the TG/GG genotype. These finding suggest that such molecular mechanisms may affect HCC recurrence.

therefore, we investigated the association between the *IL-28B* genotype and clinical outcome after initial curative treatment of HCC and clarified the molecular features in relation to the *IL-28B* genotype.

Materials and Methods

Patients

A total of 852 patients were admitted to the Department of Gastroenterology, Kanazawa University Hospital, Kanazawa, Japan between January 2000 and March 2012 for the treatment of developed HCC. The major background liver disease was hepatitis C virus (HCV; $n = 502$), followed by hepatitis B virus ($n = 148$). Treatment of HCC included surgical resection in 175 patients and RFA in 390 patients. The choice of treatment procedure was determined according to the extent of the tumor and the hepatic functional reserve as assessed by Child's classification that forms the Japanese HCC Guidelines (16, 17). In some cases indicated for surgical resection, we conducted RFA on patients who refused surgical resection, and we consequently excluded these patients on the basis of Japanese HCC guidelines.

Study inclusion criteria were: (i) Child–Pugh class A or B; (ii) the presence of up to 3 tumors, each 3 cm or less; (iii) HCV infection (positive for HCV RNA, patients with sustained viral response were excluded); (iv) radical treatment by either surgical resection or RFA; and (v) availability of blood samples for genetic analyses (Supplementary Fig. S1). Consequently, 183 patients were studied and their baseline characteristics are reported in Table 1. Informed consent was obtained from all patients before therapy. The experimental protocol was approved by the Human Genome, Gene Analysis Research Ethics Committee of Kanazawa University (Approval No. 260), and the study was conducted in accordance with the Declaration of Helsinki.

Diagnosis of HCC

HCC diagnosis was based predominantly on image analysis. Patients underwent dynamic computed tomography (CT) and/or dynamic MRI and abdominal angiography with CT imaging in the arterial and portal flow phase. HCC was diagnosed if a liver nodule showed hyperattenuation in the arterial phase and washout in the portal or delayed phase or showed typical hypervascular staining on digital subtraction angiography (18).

Table 1. Clinical features of 183 patients with HCC at entry by *IL-28B* genotype

Variables	*IL-28B* TT genotype ($n = 124$)	*IL-28B* TG/GG genotype ($n = 59$)	*P*
Sex (male:female)	76:48	32:27	0.422
Age, y (≤70:>70)	64:60	32:27	0.754
Platelet count ($\times 10^4/mm^3$; ≤10:>10)	68:56	28:31	0.429
ALT, IU/L (≤40:>40)	44:80	25:34	0.416
γ-GTP, IU/L (≤50:>50)	46:78	21:38	0.871
Albumin, g/dL (≤3.5:>3.5)	41:83	12:47	0.084
Protrombin activity, % (≤70:>70)	28:96	9:50	0.325
Total bilirubin, mg/dL (≤2:>2)	7:117	1:58	0.440
Child–Pugh class (A:B)	77:29	43:10	0.352
Therapy (resection: RFA)	19:105	10:49	0.830
Period of therapy (2000-05:2006-12)	41:83	21:38	0.741
History of IFN therapy (yes:no)	56:68	26:33	0.999
Tumor number (solitary: 2–3)	80:44	42:17	0.406
Tumor size, mm (≤20:>20)	83:41	36:23	0.508
AFP, ng/mL (≤20:>20)	60:64	37:22	0.082
DCP, AU/L (≤40:>40)	75:49	39:20	0.516

Method of treatment

Hepatic resection was carried out under intraoperative ultrasonographic monitoring and guidance. Anatomic resection was conducted in 9 patients and nonanatomic resection was conducted in 20 patients. Curative resection was defined as removal of all recognizable tumors with a clear margin (19). RFA was conducted using either the radiofrequency interstitial tumor ablation system (RITA; RITA Medical Systems Inc.) or the cool-tip system (Tyco Healthcare Group LP). All procedures were conducted according to the manufacturer's protocol. In the case of RFA, dynamic CT was conducted 1 to 3 days after therapy and the ablated area was evaluated. Complete ablation was defined as no enhancement in the ablated area on the dynamic CT. When complete ablation was not achieved, additional ablation was considered.

Follow-up

All patients were followed up by ultrasound and contrast enhancement 3-phase CT or MRI every 3 months. Local tumor progression was defined as the reappearance of tumor progression adjacent to the treated site and distant recurrence as the emergence of one or several tumor(s) not adjacent to the treated site. Patients with confirmed recurrence received further treatment such as resection, RFA, transarterial chemoembolization, and chemotherapy depending on the condition. Time to recurrence (TTR) was defined as the period from the date of therapy until the detection of tumor recurrence, death, or the last follow-up assessment. For TTR analysis, the data were censored for patients without signs of recurrence.

Genetic variation of the *IL-28B* polymorphism

Genomic DNA was extracted from peripheral blood samples using the QIAamp DNA Blood Mini Kit (Qiagen) according to the manufacturer's instructions. An *IL-28B* SNP (rs8099917) was determined using TaqMan Pre-Designed SNP Genotyping Assays as described previously (12). A custom assay was created by Applied Biosystems for rs12979860. We determined *IL-28B* genetic variations in all patients included in this study.

Affymetrix genechip analysis

Resected cancer and noncancerous liver tissue specimens were immediately frozen in liquid nitrogen and kept at −80°C until required for RNA preparation. Liver tissue RNA was isolated using the RNeasy Mini Kit (Qiagen) according to the manufacturer's instructions. Isolated RNA was stored at −70°C until required. The quality of isolated RNA was estimated after electrophoresis using an Agilent 2001 Bioanalyzer. Microarray analysis using an Affymetrix Human 133 Plus 2.0 microarray chip was conducted as described previously (13). The microarray data have been submitted to the Gene Expression Omnibus (GEO) public database at National Center for Biotechnology Information (NCBI, Bethesda, MD; accession number GSE41804).

Gene set enrichment analysis

Affymetrix GeneChip array data were normalized, preprocessed, and analyzed using R (20) and Bioconductor (21) software. Raw CEL file data were normalized using the MAS 5.0 algorithm as implemented in the *affy* package. Normalized data were $\log_2$ transformed and assessed using gene set enrichment analysis (GSEA), which is a bioinformatics method to assess whether genes with known biological/molecular function are concomitantly upregulated or downregulated in a certain gene expression dataset (22). GSEA was conducted using a parametric analysis of gene set enrichment (PAGE; ref. 23). The Gene Ontology gene set collection C5 of the Molecular Signatures Database (22) was downloaded from the Broad Institute and loaded into the R environment.

We also investigated the gene set differentially expressed HCC-infiltrating mononuclear inflammatory cells studied previously (24). *Z* scores and *P* values of all gene sets were calculated using the *PGSEA* package and an estimate was made as to whether certain gene sets, and therefore functional gene categories, were differentially regulated in HCC tissue from patients with the *IL-28B* TT genotype and the *IL-28B* TG/GG genotype.

Hierarchical clustering

Hierarchical clustering was conducted with Cluster software using Pearson's correlation distance metric and average linkage followed by visualization in Treeview software.

Histologic liver analysis

Noncancerous liver tissue that had been surgically resected from patients with HCC and liver specimens obtained by needle biopsy from the background liver of patients with HCC were fixed in 10% buffered formalin and embedded in paraffin. Each paraffin-embedded specimen was sliced into 3 to 4 μm sections and stained with hematoxylin and eosin. Each specimen was semiquantitatively analyzed by assigning a score according to each of the following features: (i) severity of inflammatory cell infiltration (0 for none, 1 for minimal, 2 for mild, 3 for moderate, and 4 for severe) in the periportal, intralobular, and portal areas; (ii) the severity of the F stage of fibrosis (0 for F0, 1 for F1, 2 for F2, 3 for F3, and 4 for F4; ref. 25); the degree of lymphoid aggregates in the portal area (0 for none, 1 for mild, 2 for scattered, 3 for clustered, 4 for lymph follicle without germinal center, and 5 for lymph follicle with germinal center); the severity of portal sclerotic change, perivenular fibrosis, and pericellular fibrosis (on a scale of 0–4 with 0 for none to 4 for severe); the severity of damage to the bile duct (on a scale of 0–4 with 0 for none to 4 for disappearance); the existence of bridging necrosis (0 for none and 1 for existence); the severity of irregular regeneration of hepatocytes as described previously (on a scale of 0–4 with 0 for none to 4 for severe; ref. 26); the grade of steatosis (on a scale of 0–4 with 0 for none to 4 for severe). The irregular regeneration score was based on the findings of a map-like distribution, anisocytosis, and pleomorphism

of the hepatocytes, bulging of the regenerated hepatocytes and proliferation of atypical hepatocytes and oncocytes.

Immunohistochemistry

Paraffin-embedded specimens were sliced into 3 to 4 μm sections, deparaffinized, and subjected to heat-induced epitope retrieval at 98°C for 40 minutes. After blocking endogenous peroxidase activity using 3% hydrogen peroxide, the slide was incubated with appropriately diluted primary antibodies. Antihuman CD4, antihuman CD8 and antihuman CD14 mouse monoclonal antibodies were used to evaluate the immunoreactivity of HCC using a DAKO EnVision+TM kit, as described in the manufacturer's instructions.

We semiquantitatively analyzed tumor tissues by assigning a score to the severity of CD4-positive and CD8-positive lymphocyte infiltration in the tumor tissue (0 for none, 1 for mild, 2 for moderate, and 3 for severe).

Statistical analysis

Fisher exact probability test was used to compare categorical variables and the Mann–Whitney *U* test was used to compare continuous variables; a *P* value of less than 0.05 was considered statistically significant. The TTR survival curve was analyzed using the Kaplan–Meier curve and compared by the log-rank test. Univariate Cox regression analysis was conducted to identify TTR predictors out of clinical and biologic parameters [sex, age, *IL-28B* genotype, therapy, platelet count, alanine aminotransferase (ALT), γ-GTP, albumin, prothrombin activity, bilirubin, Child–Pugh class, history of IFN therapy, AFP, and des-γ-carboxy prothrombin (DCP)] and tumor factors (size and number).

Multivariate analysis was conducted using the Cox regression model with backward elimination (27). The significance level for removing a factor from the model was set to 0.05. A bootstrap technique was applied to confirm the choice of variables (27). One thousand bootstrap samples were generated using resampling with replacement and Cox regression analysis with backward elimination was applied to each sample. The percentage of samples (from the total of 1,000) for which each variable was included in the model was calculated. In multivariate analysis, we evaluated two models that contained either Child–Pugh class or its components to avoid multicollinearity. Data analysis was conducted with R software. We used functions from the Regression Modeling Strategies library for validation with the bootstrap technique (28).

Results

Patient characteristics and *IL-28B* genotype frequency

We genotyped 183 patients with HCC for the *IL-28B* rs8099917 TT, TG, and GG genotypes and observed respective proportions of 67.8% (124 of 183), 30.6% (56 of 183), and 1.6% (3 of 183), which is a similar distribution to that observed in several Japanese studies of patients with CHC (13, 14, 29, 30). Although the prevalence of the TG/GG genotype was higher than that of the general population (12%–16%; refs. 12, 31, 32), there was no significant difference between our result and that of HCV-infected patients in a previous study. There was also no significant difference in clinical variables between the TT and TG/GG genotypes (Table 1).

We next genotyped 160 of 183 cases for rs12979860 and our findings were largely in concordance with those of rs8099917, with the exception of 1 case (0.6%). The haplotype of the case showed that rs8099917 was TT and rs12979860 was CT suggesting that these 2 loci are in a haplotype block with a high level of linkage disequilibrium, as previously reported (13, 30). Genotype distribution analysis showed that rs8099917 was in Hardy–Weinberg equilibrium, so we selected it for further investigation.

During the median follow-up period of 2.5 years (range, 0.3–7.2 years), 118 of 183 patients developed HCC recurrence. Local tumor progression was seen in 13 patients treated by RFA and in only 1 patient treated by resection. The local tumor progression rate and distant recurrence rate were 2.6% and 21.2% in the first year and 8.3% and 54.2% within 2.5 years, respectively. These results are comparable with previous reports by others (33, 34). The type of recurrence was also comparable between *IL-28B* genotype groups.

Associations between the *IL-28B* genotype and HCC clinical outcome

HCC TTR was also analyzed using multivariate Cox regression analysis using 15 clinical parameters and the *IL-28B* genotype. With a significance level of 0.05 for removing a variable in a Cox regression with backward elimination, the *IL-28B* genotype was selected as the final model (Table 2). To confirm this decision, a bootstrapping technique was applied. The percentages of inclusion among the 1,000 samples created by the bootstrapping technique for variables are shown in Table 2. The percentage of inclusion for the *IL-28B* genotype was 80.4%. Frequencies of another variable were lower than 40%. The bootstrap procedure result confirmed the variables chosen for the final model.

In univariate Cox regression analyses, the *IL-28B* genotype was associated with HCC recurrence (Table 2). The TTR survival curve was analyzed using the Kaplan–Meier curve and log-rank test (Fig. 1), and patients with the *IL-28B* TT genotype showed a significantly shorter median TTR (1.61 years) than those with the *IL-28B* TG/GG genotype (2.58 years; $P = 0.007$).

Histologic analysis of noncancerous liver tissues of *IL-28B* TT and TG/GG genotypes

To clarify the molecular mechanism influencing HCC recurrence, we histologically analyzed 141 noncancerous liver tissues according to previously published criteria (Table 3; ref. 26). The mean score of the degree of inflammatory cell infiltration in the periportal area was significantly higher in TT genotype patients (2.804) than TG/GG genotype patients (2.513; $P = 0.025$); the degree of inflammatory cell infiltration in the intralobular area was also

Table 2. Cox regression analysis and relative frequency of variables inclusion with $P < 0.05$ (in 1,000 bootstrap samples)

Variables	Univariate		Multivariate		Frequency (%)
	HR (95% CI)	*P*	HR (95%CI)	*P*	
IL-28B allele: major vs. minor	2.674 (1.161–2.627)	0.007	2.674 (1.161–2.627)	0.007	80.4
Tumor size, mm: >20 vs. ≤20	1.303 (0.881–1.880)	0.193			39.8
AFP, ng/mL: >20 vs. ≤20	1.674 (0.948–1.968)	0.094			33.2
γ-GTP, IU/L: >50 vs. ≤50	1.188 (0.865–1.804)	0.235			32.8
Therapy: RFA vs. resection	1.218 (0.826–2.266)	0.223			31.6
DCP, AU/L: >40 vs. ≤40	1.524 (0.920–1.945)	0.127			27.4
ALT, IU/L: >40 vs. ≤40	0.277 (0.721–1.544)	0.782			23.6
Child–Pugh class: A vs. B	0.025 (0.653–1.515)	0.980			19.2
Period of therapy: 2000-05 vs. 2006-12	0.886 (0.818–1.701)	0.375			15.8
History of IFN therapy: yes vs. no	0.570 (0.771–1.605)	0.569			15.8
Sex: male vs. female	0.108 (0.697–1.496)	0.914			14.6
Tumor number: solitary vs. 2-3	0.263 (0.845–1.857)	0.263			13.4
Platelet count ($\times 10^4/mm^3$): >10 vs. ≤10	0.118 (0.680–1.407)	0.906			12.6
Age: per 1 y	0.621 (0.986–1.028)	0.534			8.4

higher in the TT genotype (2.522) than the TG/GG genotype (2.308), although this did not reach statistical significance ($P = 0.08$). Furthermore, the mean score of the degree of hepatocyte anisocytosis was significantly higher in the TT genotype (1.891) than the TG/GG genotype (1.385; $P = 0.024$). Anisocytosis is characterized by viability of cell size with focal dysplastic change and indicates irregular regeneration of hepatocytes. The irregular regeneration score was higher in the TT genotype (2.207) than the TG/GG genotype (1.795), albeit not significantly ($P = 0.105$).

IL-28B TT and TG/GG genotype gene expression profiles in the noncancerous liver

We next compared the gene expression profile of HCC tissues and noncancerous liver tissues of both the *IL-28B* TT and *IL-28B* TG/GG genotype. Ten patients with HCC were selected from each *IL-28B* genotype and their gene expression was determined using Affymetrix genechip analysis (Supplementary Table S1). We recently reported that expression of hepatic ISGs is downregulated in individuals with the *IL-28B* TT genotype, whereas the expression of other immune response-related genes was shown to be upregulated (13). Therefore, to validate our expression data, we compared the expression of ISGs and other immune response-related genes in the present study with that of the previous study. We analyzed the expression data of 20 patients from the current study in addition to another series of 91 patients with CHC from our previous study.

One-way hierarchical clustering using 28 representative ISGs showed that patients with the *IL-28B* TG/GG genotype

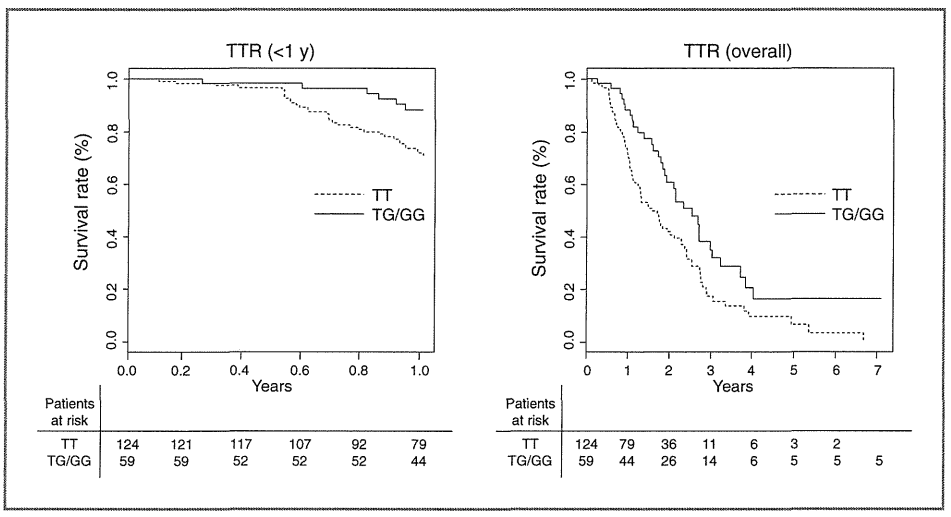

Figure 1. Kaplan–Meier curves of early and overall TTR in relation to *IL-28B* genotype. The patients with the *IL-28B* TT genotype showed a significantly shorter median TTR (1.61 years) than those with the *IL-28B* TG/GG genotype (2.58 years; $P = 0.007$).

Table 3. Comparison of liver histology between *IL-28B* major and minor genotypes

Variable	*IL-28B* TT genotype ($n = 92$)	*IL-28* TG/GG genotype ($n = 39$)	*P* value
Score of inflammatory cell infiltration			
Periportal	2.804	2.513	0.032
Intralobular	2.522	2.308	0.082
Portal	2.946	2.846	0.322
Fibrosis	3.587	3.436	0.428
Portal lymphoid reaction	4.098	3.949	0.363
Damage of bile duct	0.380	0.256	0.216
Portal sclerotic change	0.076	0.077	0.990
Perivenular fibrosis	1.133	1.000	0.447
Pericellular fibrosis	1.163	0.821	0.045
Bridging fibrosis	0.957	0.641	0.106
Irregular regeneration	2.207	1.795	0.105
Anisocytosis	1.891	1.385	0.024
Bulging	0.326	0.436	0.485
Map-like distribution	1.370	1.333	0.881
Oncocytes	1.326	1.051	0.227
Nodularity	1.185	1.231	0.849
Atypical hepatocytes	0.467	0.692	0.304
Steatosis	1.707	1.692	0.951

NOTE: Data shown as mean.

had higher expression of hepatic ISGs, whereas patients with the TT genotype showed lower expression of hepatic ISGs in CHC tissues and noncancerous background liver tissue, confirming our previous data (Fig. 2A and Supplementary Table S2). Expression of hepatic ISGs in HCC tissues was lower than in background liver tissues, with no relationship to the *IL-28B* genotype. Hierarchical clustering of 51 representative immune response-related genes from the Gene Ontology gene set of the Molecular Signatures Database indicated that their expression was upregulated in TT genotype compared with TG/GG genotype tissues, with the exception of HCC tissues (Fig. 2B and Supplementary Table S2). Upregulation of immune response-related genes suggests that hepatic inflammation is more severe in TT genotype patients, which is consistent with our histologic findings and recent studies that reported an association between high serum ALT levels and the *IL-28B* TT genotype (14, 29).

Gene expression profile of HCC tissues from *IL-28B* TT and TG/GG genotypes

We applied PAGE to identify gene sets differentially regulated between the different *IL-28B* genotypes from the whole gene expression profiles derived from HCC tissues. Analysis of groups of genes involved in a specific function enables significant differences to represent a biologically meaningful result (23). Many gene sets associated with the immune system (e.g., the immune system process, T-cell activation, regulation of T-cell activation, and T-cell proliferation) showed a significant increase in their expression in patients with HCC with the *IL-28B* TG/GG genotype (Supplementary Table S3). This PAGE profile was consistent with the hierarchical clustering of 51 immune response-related genes (Fig. 2B) and suggests that the immune response to tumors might be more intensive in *IL-28B* TG/GG genotype HCC than *IL-28B* TT genotype HCC.

Lymphocyte infiltration into HCC tissues with the *IL-28B* TG/GG genotype

To verify our PAGE profile, we histologically compared HCC tissue of 20 cases of the *IL-28B* TT genotype and 12 cases of the TG/GG genotype using immunohistochemical staining with antibodies against helper T cells (CD4) and cytotoxic T cells (CD8). The mean score of the degree of $CD8^+$ lymphocyte infiltration in the tumor tissue was significantly higher in the TG/GG genotype (1.75) than the TT genotype (1.175; $P = 0.047$; Supplementary Table S4). A representative case is shown in Fig. 3. There was no morphologic alteration associated with the *IL-28B* genotype. Immunohistochemical analysis showed intratumoral infiltration of $CD4^+$ and $CD8^+$ lymphoid cells and slight infiltration of monocytes/macrophages in HCC of the *IL-28B* TG/GG genotype, compared with little infiltration of lymphocytes or monocytes/macrophages in HCC of the *IL-28B* TT genotype.

Furthermore, the gene set differentially expressed in HCC-infiltrating mononuclear inflammatory cells from our previous study (24) was upregulated in HCC of the *IL-28B* TG/GG genotype (Z score, -9.879; $P < 0.001$). One-way hierarchical clustering was carried out of 122 genes involved in the gene set differentially expressed in HCC-infiltrating

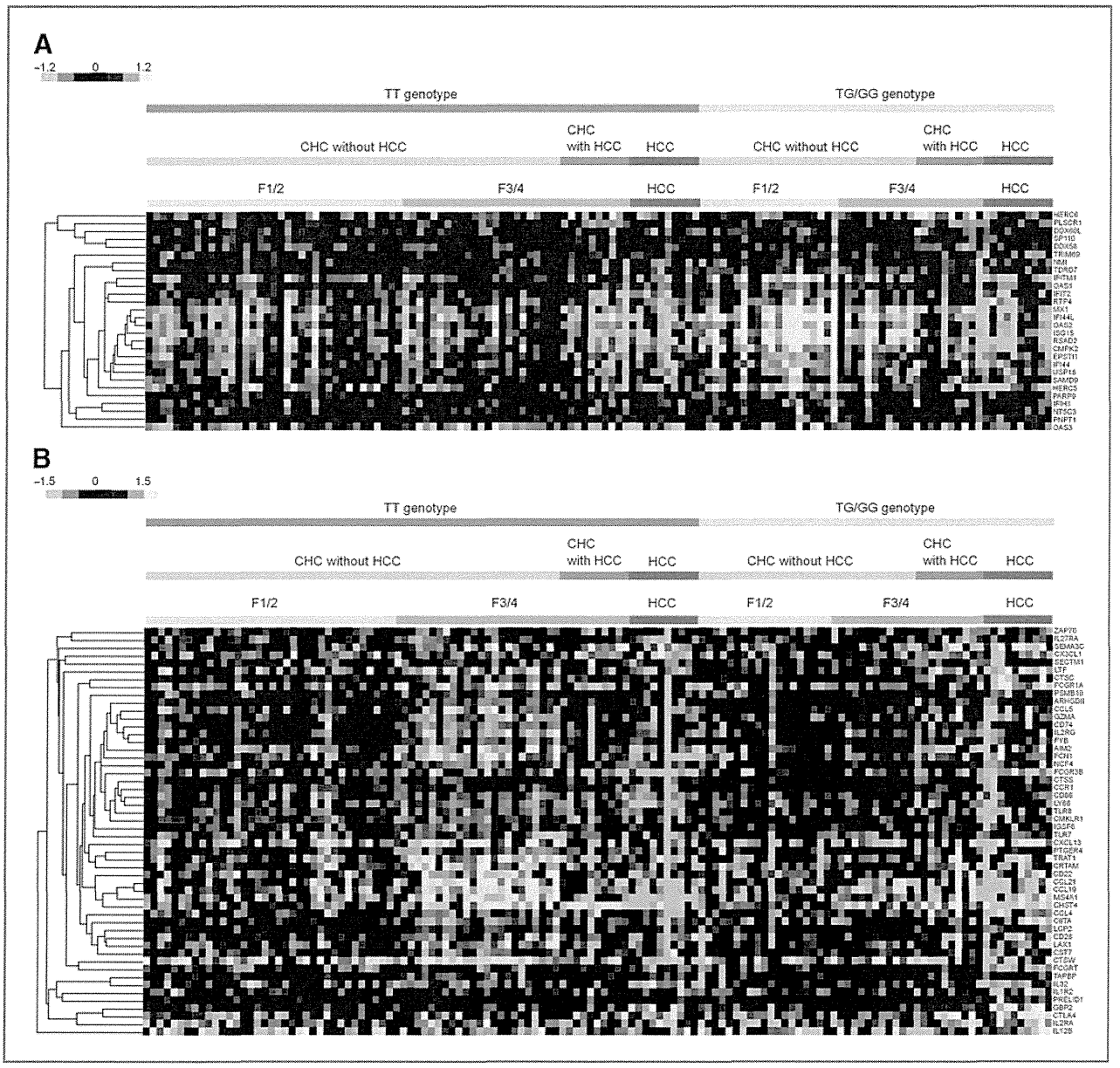

Figure 2. A, one-way hierarchical clustering of 28 representative ISGs of 111 patients with the *IL-28B* genotype. B, one-way hierarchical clustering analysis of 51 representative immune response-related genes of 111 patients with the *IL-28B* genotype.

mononuclear inflammatory cells. Most of the 122 genes were expressed at high levels in many HCC tissues of *IL-28B* TG/GG genotype patients (Supplementary Fig. S2).

Discussion

IL-28B is a recently identified, novel IFN-λ family member that shares the same biologic properties as type I IFNs (9). Recent reports have shown a significant association between *IL-28B* allelic variants and treatment outcome in CHC (11, 12). *IL-28B* genotyping is therefore considered to be a suitable pretreatment predictor of treatment response for individual patients, and also an indicator of biochemical and histologic findings in patients infected with HCV (14). In this study, we determined that the *IL-28B* genotype is associated with HCC recurrence in patients with CHC as patients with the *IL-28B* TT genotype showed a significantly higher incidence of recurrence than those with the *IL-28B* TG/GG genotype after curative therapy. To our knowledge, this is the first study to reveal an association between the *IL-28B* genotype and HCC recurrence and molecular features in patients with CHC.

To date, there are several contradicting results about the association of the *IL-28B* genotype and progression of liver disease including the development of HCC. Fabris and colleagues and Eurich and colleagues reported that

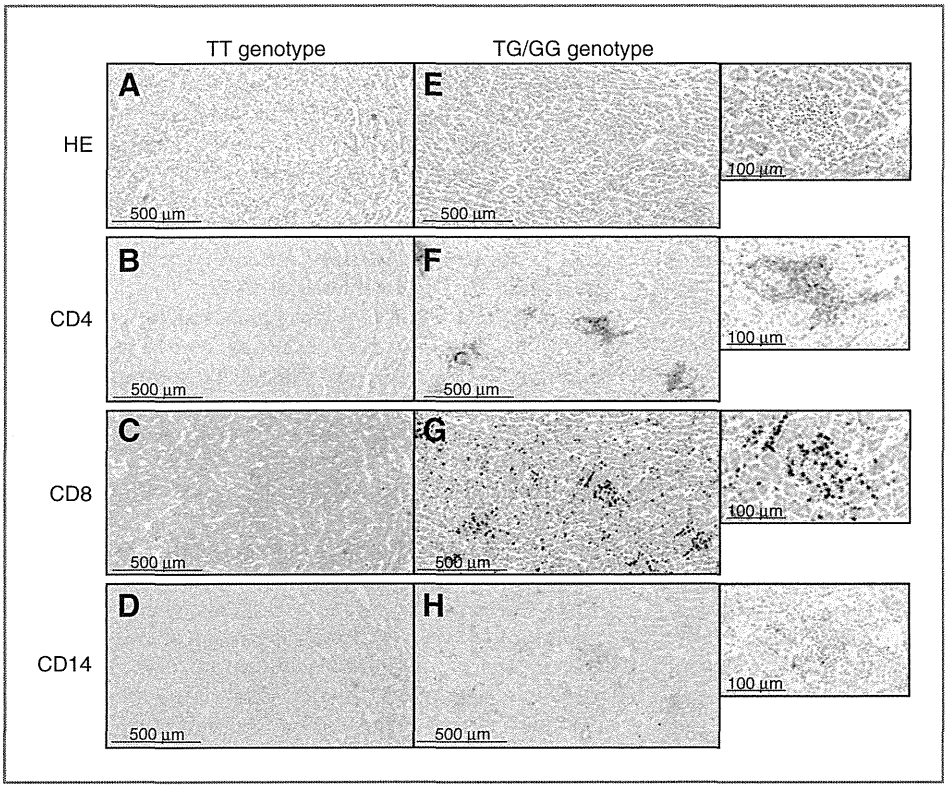

Figure 3. Expression of CD4, CD8, and CD14 in tumor-infiltrating mononuclear cells in HCC tissues. Immunohistochemical analysis of noncancerous liver tissues of *IL-28B* TT (A–D) and TG/GG genotypes (E–H). Samples were analyzed by hematoxylin and eosin staining (A and E), CD4 staining (B and F), CD8 staining (C and G), and CD14 staining (D and H).

patients with a T allele in rs12979860 (G allele in rs8099917) were at a high risk of progressing to liver cirrhosis and HCC (35, 36), however, these reports have not yet been confirmed by others. A large-scale European genome-wide association study (GWAS) recently identified a weak protective role for the rs12979860 T allele in the progression of fibrosis during HCV infection (37), whereas a Japanese GWAS identifying a susceptibility locus for HCV-induced HCC found no association of rs12979860 and rs8099917 SNPs with HCC (38). In support of these findings, Joshita and colleagues reported no association between the *IL-28B* genotype and the incidence of primary HCC (39). These results show a good concordance with those of the present study, which revealed that the *IL-28B* genotype was not associated with HCC incidence before treatment (Table 1). Furthermore, closer histologic assessment showed a high score of periportal inflammation and pericellular fibrosis in the rs8099917 TT genotype (CC in rs12979860). This suggests that our patient selection process was not biased, and that our results are in agreement with the Japanese study and are comparable with the European study.

To date, the reasons for contradicting results about the association of the *IL-28B* genotype and progression of liver disease have not been clear, however, clinical bias such as patient number, history of treatment, virus genotype, and titer and racial differences may affect the results. It should be noted that significant differences in genotype frequencies with respect to ethnic/racial groups have previously been reported for *IL-28B* SNPs (11). To overcome these limitations, a future cross-sectional prospective study should be conducted.

Several risk factors for HCC recurrence have previously been reported, including the presence of cirrhosis, high AFP levels, and multiplicity of tumors 7, 8). However, multivariate analysis and the bootstrap procedure of the present study revealed that the *IL-28B* genotype was independent indicators for recurrence, suggesting that it is stronger predictors of HCC recurrence than other factors.

The expression of hepatic ISGs was higher in *IL-28B* TG/GG genotype patients than *IL-28B* TT genotype patients with CHC in this study. This confirms our previous findings in a different cohort and those of another research group (13, 40). Several ISGs have been reported to have antiproliferative and proapoptotic functions (41, 42), and IFN-α (type I IFN) has also been found to inhibit metastasis and human HCC recurrence after curative resection mediated by angiogenesis (43). Indeed, *IL-28B* rs8099917 is associated with early HCC recurrence (<1 year), possibly because of the intrahepatic metastasis of HCC in this study (Fig. 1 and Supplementary Table S5). These reports and our findings suggest that high expression of hepatic ISGs might cause the low HCC recurrence in the *IL-28B* TG/GG genotype, although the mechanism of this association remains unknown.

Microarray, histologic, and immunohistochemical analysis in the present study showed that the immune response was more severe in chronic hepatitis and noncancerous tissue of *IL-28B* TT genotype compared with TG/GG genotype patients. Serum ALT levels were also higher in the

IL-28B TT genotype, albeit not significantly. These results support previous findings that showed higher serum ALT levels and more severe liver inflammation in TT genotype compared with TG/GG genotype patients with HCC (14, 29). Irregular regeneration of hepatocytes develops as a result of repeated cycles of necrosis and regeneration of hepatocytes and was previously reported to be an important predictive factor for the development of HCC (26). We histologically showed that the degree of hepatocyte anisocytosis was more severe in noncancerous livers of TT genotype than TG/GG genotype patients, perhaps because of *IL-28B* genotype-dependent hepatic inflammation. This might also affect the late recurrence of HCC (>1 year) as a result of the multicentric occurrence of HCC in background liver disease. In the late recurrence group, *IL-28B* TT genotype patients showed a shorter TTR than *IL-28B* TG/GG genotype patients although this did not reach statistical significance ($P = 0.086$; Supplementary Fig. S3; Supplementary Table S6).

Previous studies showed that the gene expression profile of noncancerous liver tissue was associated with late recurrence HCC and the multicentric occurrence of HCC (44). However, the gene set expression of these studies did not differ between the *IL-28B* TT and TG/GG genotypes in the present study. Although the reason for this discrepancy is unclear, the *IL-28B* genotype may affect early recurrence more than late recurrence, and the limited number of patients and the short follow-up period may affect statistical comparisons. Therefore, further investigations with a large series of patients are necessary to clarify whether *IL-28B* genotype-dependent inflammation influences HCC recurrence.

On the other hand, the gene expression profile and histologic analyses showed that more lymphocytes infiltrate into the tumor tissue of the *IL-28B* TG/GG genotype than the TT genotype. Chew and colleagues previously showed that 14 intratumoral immune gene signatures were able to identify molecular cues driving the tumor infiltration of lymphocytes and predict the survival of patients with HCC, particularly during the early stages of disease (45). We can confirm that the expression of some of these 14 genes was higher in TG/GG genotype than TT genotype patients (Supplementary Fig. S4), supporting the association of the *IL-28B* genotype, HCC recurrence, and histologic findings. The presence of lymphocyte infiltration in HCC was also reported as a negative predictor of HCC recurrence after liver transplantation (46), and this phenomenon may contribute to a lower incidence of HCC recurrence in the TG/GG genotype.

It may seem contradictory that the immune response in noncancerous liver was more severe in TT genotype than TG/GG genotype patients despite the fact that the expression of immune genes was higher in tumor tissue and more lymphocytes infiltrated the tumor in the TG/GG genotype compared with the TT genotype. Although we are unable to explain this contradiction, it is conceivable that the host immune reaction has a differential role between tumor and nontumor tissue. Moreover, HCV-specific T-cell immune responses, which are essential for disease control, are attenuated in patients with CHC, and T-cell exhaustion has recently been implicated in the deficient control of chronic viral infections. On the other hand, little is known on self- and tumor-specific T-cell responses in patients with HCC. While several reports have shown the existence of exhausted T cells in a tumor environment, impaired T-cell responses to tumors are unlikely to be simply explained by T-cell exhaustion (47).

Anergy or other functional statuses such as suppressive immunity by tumor cells should be considered in tumor immunity. Therefore, differences in immunity to viral antigens and self- and tumor-antigens could explain our findings, although further work should be carried out to confirm these conclusions. We have preliminarily confirmed that the ratio of regulatory T cells is higher in the peripheral blood of *IL-28B* TT genotype HCC patients than *IL-28B* TG/GG genotype patients, although there is no significant difference between non-HCC *IL-28B* TT genotype and *IL-28B* TG/GG genotype patients (data not shown). Although the cause of this phenomenon is unclear, our gene expression profile of noncancerous liver and tumor tissues suggests paradoxical roles for the immune response in CHC and HCC depending on *IL-28B* genotype; it will be necessary to clarify these mechanisms in future investigations.

Recently, a sustained virologic response (SVR) to CHC antiviral treatment was shown to be associated with a lower risk of HCC recurrence (48). Although we did not include patients with SVR in the current study, we nevertheless observed that they showed a longer recurrence-free survival than patients infected with HCV, independent of *IL-28B* genotype (data not shown). This result together with the association between the *IL-28B* genotype and response to antiviral treatment promotes recommendations for aggressive CHC antiviral treatment, especially in cases with the *IL-28B* TT genotype.

RFA is a recently developed technique and its efficacy has been reported equal to that of surgical resection, especially in early-stage HCC (3–6). In the European Association for the Study of the Liver–European Organisation for Research and Treatment of Cancer (EASL-EORTC) guidelines, RFA is considered the standard care for patients with Barcelona Clinic Liver Cancer stage 0-A tumors not suitable for surgery and whether or not RFA can be considered a competitive alternative to resection is uncertain (49). In our study, the local tumor progression rate was not statistically different between RFA and resection cases. However, further studies with an appropriate sample population are necessary to clarify the comparison of RFA and resection. The present study has some limitations. It was a retrospective cohort and a single-center study, so it was difficult to completely eliminate bias. Further prospective studies of a larger series of patients should be conducted to validate our results. As a consequence of the small sample size and even smaller number of patients undergoing surgical resection, we could not show an association between *IL-28B* genotype and HCC

recurrence in the surgical resection group (data not shown). However, we did find no significant difference in TTR between RFA and surgical resection, confirming previous findings.

In conclusion, we found that the *IL-28B* rs8099917 TT genotype is associated with shorter TTR in patients with HCC with CHC. Microarray analysis showed a high expression of ISGs in background liver and high expression of immune system-related genes in tumor tissues of the *IL-28B* TG/GG genotype. Histologic findings also showed that more lymphocytes infiltrated into tumor tissues in the TG/GG genotype. The *IL-28B* genotype therefore is a candidate useful genetic marker to predict HCC recurrence as well as the response to pegylated-IFN and ribavirin combination therapy for CHC.

Disclosure of Potential Conflicts of Interest

No potential conflicts of interest were disclosed.

Authors' Contributions

Conception and design: M. Honda, Y. Sakai, M. Moriyama, S. Kaneko
Development of methodology: M. Moriyama
Acquisition of data (provided animals, acquired and managed patients, provided facilities, etc.): Y. Hodo, A. Tanaka, K. Arai, T. Yamashita, T. Yamashita, A. Sakai, Y. Nakanuma, M. Moriyama, S. Kaneko
Analysis and interpretation of data (e.g., statistical analysis, biostatistics, computational analysis): Y. Hodo, M. Honda, M. Sasaki, M. Moriyama
Writing, review, and/or revision of the manuscript: Y. Hodo, M. Honda, M. Moriyama
Administrative, technical, or material support (i.e., reporting or organizing data, constructing databases): Y. Hodo, A. Tanaka, Y. Nomura, K. Arai, E. Mizukoshi, M. Sasaki, M. Moriyama, S. Kaneko
Study supervision: Y. Sakai, E. Mizukoshi, M. Moriyama

The costs of publication of this article were defrayed in part by the payment of page charges. This article must therefore be hereby marked *advertisement* in accordance with 18 U.S.C. Section 1734 solely to indicate this fact.

Received May 25, 2012; revised December 20, 2012; accepted February 7, 2013; published OnlineFirst February 20, 2013.

References

1. Yang JD, Roberts LR. Hepatocellular carcinoma: a global view. Nat Rev Gastroenterol Hepatol 2010;7:448–58.
2. Cha C, DeMatteo RP, Blumgart LH. Surgery and ablative therapy for hepatocellular carcinoma. J Clin Gastroenterol 2002;35(5 Suppl 2): S130–7.
3. Lü M, Kuang M, Liang L, Xie X, Peng B, Liu G, et al. Surgical resection versus percutaneous thermal ablation for early-stage hepatocellular carcinoma: a randomized clinical trial. Zhonghua Yi Xue Za Zhi 2006; 86:801–5.
4. Chen M-S, Li J-Q, Zheng Y, Guo R-P, Liang H-H, Zhang Y-Q, et al. A prospective randomized trial comparing percutaneous local ablative therapy and partial hepatectomy for small hepatocellular carcinoma. Ann Surg 2006;243:321–8.
5. Hong SN, Lee S-Y, Choi MS, Lee JH, Koh KC, Paik SW, et al. Comparing the outcomes of radiofrequency ablation and surgery in patients with a single small hepatocellular carcinoma and well-preserved hepatic function. J Clin Gastroenterol 2005;39: 247–52.
6. Nishikawa H, Inuzuka T, Takeda H, Nakajima J, Matsuda F, Sakamoto A, et al. Comparison of percutaneous radiofrequency thermal ablation and surgical resection for small hepatocellular carcinoma. BMC Gastroenterol 2011;11:143.
7. Koike Y, Shiratori Y, Sato S, Obi S, Teratani T, Imamura M, et al. Risk factors for recurring hepatocellular carcinoma differ according to infected hepatitis virus-an analysis of 236 consecutive patients with a single lesion. Hepatology 2000;32:1216–23.
8. Yamanaka Y, Shiraki K, Miyashita K, Inoue T, Kawakita T, Yamaguchi Y, et al. Risk factors for the recurrence of hepatocellular carcinoma after radiofrequency ablation of hepatocellular carcinoma in patients with hepatitis C. World J Gastroenterol 2005;11:2174–8.
9. Sheppard P, Kindsvogel W, Xu W, Henderson K, Schlutsmeyer S, Whitmore TE, et al. IL-28, IL-29 and their class II cytokine receptor IL-28R. Nat Immunol 2003;4:63–8.
10. Li M, Liu X, Zhou Y, Su SB. Interferon-lambdas: the modulators of antivirus, antitumor, and immune responses. J Leukoc Biol 2009; 86:23–32.
11. Ge D, Fellay J, Thompson AJ, Simon JS, Shianna KV, Urban TJ, et al. Genetic variation in IL28B predicts hepatitis C treatment-induced viral clearance. Nature 2009;461:399–401.
12. Tanaka Y, Nishida N, Sugiyama M, Kurosaki M, Matsuura K, Sakamoto N, et al. Genome-wide association of IL28B with response to pegylated interferon-alpha and ribavirin therapy for chronic hepatitis C. Nat Genet 2009;41:1105–9.
13. Honda M, Sakai A, Yamashita T, Nakamoto Y, Mizukoshi E, Sakai Y, et al. Hepatic ISG expression is associated with genetic variation in interleukin 28B and the outcome of IFN therapy for chronic hepatitis C. Gastroenterology 2010;139:499–509.
14. Abe H, Ochi H, Maekawa T, Hayes CN, Tsuge M, Miki D, et al. Common variation of IL28 affects gamma-GTP levels and inflammation of the liver in chronically infected hepatitis C virus patients. J Hepatol 2010;53:439–43.
15. Rauch A, Kutalik Z, Descombes P, Cai T, Di Iulio J, Mueller T, et al. Genetic variation in IL28B is associated with chronic hepatitis C and treatment failure: a genome-wide association study. Gastroenterology 2010;138:1338–45, 1345.e1–7.
16. Kudo M, Okanoue T. Management of hepatocellular carcinoma in Japan: consensus-based clinical practice manual proposed by the Japan Society of Hepatology. Oncology 2007;72(Suppl 1):2–15.
17. Kokudo N, Makuuchi M. Evidence-based clinical practice guidelines for hepatocellular carcinoma in Japan: the J-HCC guidelines. J Gastroenterol 2009;44(Suppl 1):119–21.
18. Matsui O. Imaging of multistep human hepatocarcinogenesis by CT during intra-arterial contrast injection. Intervirology 2004;47:271–6.
19. Liver Cancer Study Group of Japan. The general rules for the clinical and pathological study of primary liver cancer. 5th ed. Tokyo, Japan: Kanahara Shuppan; 2009.
20. R Development Core Team. R: a language and environment for statistical computing. Vienna, Austria: R Foundation for Statistical Computing; 2012. [cited 2012 May 1]. Available from: http://www.r-project.org/.
21. Gentleman RC, Carey VJ, Bates DM, Bolstad B, Dettling M, Dudoit S, et al. Bioconductor: open software development for computational biology and bioinformatics. Genome Biol 2004;5:R80.
22. Subramanian A, Tamayo P, Mootha VK, Mukherjee S, Ebert BL, Gillette MA, et al. Gene set enrichment analysis: a knowledge-based approach for interpreting genome-wide expression profiles. Proc Natl Acad Sci U S A 2005;102:15545–50.
23. Kim S-Y, Volsky DJ. PAGE: parametric analysis of gene set enrichment. BMC Bioinformatics. 2005;6:144.
24. Sakai Y, Honda M, Fujinaga H, Tatsumi I, Mizukoshi E, Nakamoto Y, et al. Common transcriptional signature of tumor-infiltrating mononuclear inflammatory cells and peripheral blood mononuclear cells in hepatocellular carcinoma patients. Cancer Res 2008;68:10267.
25. Desmet VJ, Gerber M, Hoofnagle JH, Manns M, Scheuer PJ. Classification of chronic hepatitis: diagnosis, grading and staging. Hepatology 1994;19:1513–20.

26. Ueno Y, Moriyama M, Uchida T, Arakawa Y. Irregular regeneration of hepatocytes is an important factor in the hepatocarcinogenesis of liver disease. Hepatology 2001;33:357–62.
27. Sauerbrei W, Schumacher M. A bootstrap resampling procedure for model building: application to the Cox regression model. Stat Med 1992;11:2093–109.
28. Harrell FE Jr. rms: regression modeling strategies. 2012. [cited 2012 May 1]. Available from: http://cran.r-project.org/package=rms.
29. Akuta N, Suzuki F, Hirakawa M, Kawamura Y, Yatsuji H, Sezaki H, et al. Amino acid substitution in hepatitis C virus core region and genetic variation near the interleukin 28B gene predict viral response to telaprevir with peginterferon and ribavirin. Hepatology 2010;52:421–9.
30. Miyamura T, Kanda T, Nakamoto S, Wu S, Fujiwara K, Imazeki F, et al. Hepatic STAT1-nuclear translocation and interleukin 28B polymorphisms predict treatment outcomes in hepatitis C virus genotype 1-infected patients. PLoS ONE 2011;6:e28617.
31. Ochi H, Maekawa T, Abe H, Hayashida Y, Nakano R, Imamura M, et al. IL-28B predicts response to chronic hepatitis C therapy—fine-mapping and replication study in Asian populations. J Gen Virol 2011;92: 1071–81.
32. Database of single nucleotide polymorphisms (dbSNP). Bethesda, MD: National Center for Biotechnology Information, National Library of Medicine. dbSNP accession:rs8099917 (dbSNP Build ID: 137). [cited 2012 Oct 1]. Available from: http://www.ncbi.nlm.nih.gov/SNP/.
33. Shiina S, Tateishi R, Arano T, Uchino K, Enooku K, Nakagawa H, et al. Radiofrequency ablation for hepatocellular carcinoma: 10-year outcome and prognostic factors. Am J Gastroenterol 2012;107:569–77.
34. Lencioni R, Cioni D, Crocetti L, Franchini C, Pina C Della, Lera J, et al. Early-stage hepatocellular carcinoma in patients with cirrhosis: long-term results of percutaneous image-guided radiofrequency ablation. Radiology 2005;234:961–7.
35. Fabris C, Falleti E, Cussigh A, Bitetto D, Fontanini E, Bignulin S, et al. IL-28B rs12979860 C/T allele distribution in patients with liver cirrhosis: role in the course of chronic viral hepatitis and the development of HCC. J Hepatol 2011;54:716–22.
36. Eurich D, Boas-Knoop S, Bahra M, Neuhaus R, Somasundaram R, Neuhaus P, et al. Role of IL28B polymorphism in the development of hepatitis C virus-induced hepatocellular carcinoma, graft fibrosis, and posttransplant antiviral therapy. Transplantation 2012;93:644–9.
37. Patin E, Kutalik Z, Guergnon J, Bibert S, Nalpas B, Jouanguy E, et al. Genome-wide association study identifies variants associated with progression of liver fibrosis from HCV infection. Gastroenterology 2012;143:1244–52.e12.
38. Kumar V, Kato N, Urabe Y, Takahashi A, Muroyama R, Hosono N, et al. Genome-wide association study identifies a susceptibility locus for HCV-induced hepatocellular carcinoma. Nat Genet 2011;43:455–8.
39. Joshita S, Umemura T, Katsuyama Y, Ichikawa Y, Kimura T, Morita S, et al. Association of IL28B gene polymorphism with development of hepatocellular carcinoma in Japanese patients with chronic hepatitis C virus infection. Hum Immunol 2012;73:298–300.
40. Urban TJ, Thompson AJ, Bradrick SS, Fellay J, Schuppan D, Cronin KD, et al. IL28B genotype is associated with differential expression of intrahepatic interferon-stimulated genes in patients with chronic hepatitis C. Hepatology 2010;52:1888–96.
41. Besch R, Poeck H, Hohenauer T, Senft D, Häcker G, Berking C, et al. Proapoptotic signaling induced by RIG-I and MDA-5 results in type I interferon-independent apoptosis in human melanoma cells. J Clin Invest 2009;119:2399–411.
42. Stawowczyk M, Van Scoy S, Kumar KP, Reich NC. The interferon stimulated gene 54 promotes apoptosis. J Biol Chem 2011;286: 7257–66.
43. Wang L, Wu W-Z, Sun H-C, Wu X-F, Qin L-X, Liu Y-K, et al. Mechanism of interferon alpha on inhibition of metastasis and angiogenesis of hepatocellular carcinoma after curative resection in nude mice. J Gastrointest Surg 2003;7:587–94.
44. Hoshida Y, Villanueva A, Kobayashi M, Peix J, Chiang DY, Camargo A, et al. Gene expression in fixed tissues and outcome in hepatocellular carcinoma. N Engl J Med 2008;359:1995–2004.
45. Chew V, Chen J, Lee D, Loh E, Lee J, Lim KH, et al. Chemokine-driven lymphocyte infiltration: an early intratumoural event determining long-term survival in resectable hepatocellular carcinoma. Gut 2012;61: 427–38.
46. Unitt E, Marshall A, Gelson W, Rushbrook SM, Davies S, Vowler SL, et al. Tumour lymphocytic infiltrate and recurrence of hepatocellular carcinoma following liver transplantation. J Hepatol 2006;45:246–53.
47. Baitsch L, Baumgaertner P, Devêvre E, Raghav SK, Legat A, Barba L, et al. Exhaustion of tumor-specific $CD8^+$ T cells in metastases from melanoma patients. J Clin Invest 2011;121:2350–60.
48. Miyatake H, Kobayashi Y, Iwasaki Y, Nakamura S-I, Ohnishi H, Kuwaki K, et al. Effect of previous interferon treatment on outcome after curative treatment for hepatitis C virus-related hepatocellular carcinoma. Dig Dis Sci 2012;57:1092–101.
49. European Association For The Study Of The Liver; European Organisation For Research And Treatment Of Cancer. EASL-EORTC clinical practice guidelines: management of hepatocellular carcinoma. J hepatol 2012;56:908–43.

Proteasome Dysfunction Mediates Obesity-Induced Endoplasmic Reticulum Stress and Insulin Resistance in the Liver

Toshiki Otoda,[1] Toshinari Takamura,[1] Hirofumi Misu,[1] Tsuguhito Ota,[2] Shigeo Murata,[3] Hiroto Hayashi,[1] Hiroaki Takayama,[1] Akihiro Kikuchi,[1] Takehiro Kanamori,[1] Kosuke R. Shima,[1] Fei Lan,[1] Takashi Takeda,[1] Seiichiro Kurita,[1] Kazuhide Ishikura,[1] Yuki Kita,[1] Kaito Iwayama,[4] Ken-ichiro Kato,[1] Masafumi Uno,[1] Yumie Takeshita,[1] Miyuki Yamamoto,[5] Kunpei Tokuyama,[4] Shoichi Iseki,[5] Keiji Tanaka,[6] and Shuichi Kaneko[1]

Chronic endoplasmic reticulum (ER) stress is a major contributor to obesity-induced insulin resistance in the liver. However, the molecular link between obesity and ER stress remains to be identified. Proteasomes are important multicatalytic enzyme complexes that degrade misfolded and oxidized proteins. Here, we report that both mouse models of obesity and diabetes and proteasome activator (PA)28-null mice showed 30–40% reduction in proteasome activity and accumulation of polyubiquitinated proteins in the liver. PA28-null mice also showed hepatic steatosis, decreased hepatic insulin signaling, and increased hepatic glucose production. The link between proteasome dysfunction and hepatic insulin resistance involves ER stress leading to hyperactivation of c-Jun NH_2-terminal kinase in the liver. Administration of a chemical chaperone, phenylbutyric acid (PBA), partially rescued the phenotypes of PA28-null mice. To confirm part of the results obtained from in vivo experiments, we pretreated rat hepatoma-derived H4IIEC3 cells with bortezomib, a selective inhibitor of the 26S proteasome. Bortezomib causes ER stress and insulin resistance in vitro—responses that are partly blocked by PBA. Taken together, our data suggest that proteasome dysfunction mediates obesity-induced ER stress, leading to insulin resistance in the liver. ***Diabetes* 62:811–824, 2013**

Obesity is a major cause of insulin resistance and contributes to the development of type 2 diabetes (1). Growing evidence suggests that chronic endoplasmic reticulum (ER) stress in the liver is a major contributor to obesity-induced insulin resistance (2–4). However, the molecular mechanisms linking obesity and ER stress are not fully understood.

From the [1]Department of Disease Control and Homeostasis, Kanazawa University Graduate School of Medical Sciences, Ishikawa, Japan; the [2]Frontier Science Organization, Kanazawa University, Ishikawa, Japan; the [3]Laboratory of Protein Metabolism, Department of Integrated Biology, Graduate School of Pharmaceutical Sciences, University of Tokyo, Tokyo, Japan; the [4]Graduate School of Comprehensive Human Science, University of Tsukuba, Tsukuba, Japan; the [5]Department of Histology and Embryology, Kanazawa University Graduate School of Medical Sciences, Ishikawa, Japan; and the [6]Laboratory of Protein Metabolism, Tokyo Metropolitan Institute of Medical Science, Tokyo, Japan.

Corresponding author: Toshinari Takamura, ttakamura@m-kanazawa.jp.

Received 25 November 2011 and accepted 9 October 2012.

DOI: 10.2337/db11-1652

This article contains Supplementary Data online at http://diabetes.diabetesjournals.org/lookup/suppl/doi:10.2337/db11-1652/-/DC1.

T.Oto. and T.Taka. contributed equally to this work.

See accompanying commentary, p. 691.

We previously identified metabolic pathways that are significantly altered by obesity in the livers of people with type 2 diabetes by analyzing comprehensive gene expression profiles using DNA chips (5). We found that genes involved in ubiquitin-proteasome pathways were coordinately upregulated in obese individuals. Proteasomes play fundamental roles in processes that are essential for cell viability (6).

Eukaryotic cells contain several types of proteasomes. Core 20S proteasomes (20S) have binding sites for the regulatory particles proteasome activator (PA)700 and PA28 (7). PA700–20S-PA700 complexes are known as 26S proteasomes and are ATP-dependent machines that degrade cell proteins (7). PA28 is found in both previously described PA28–20S-PA28 complexes and PA700–20S-PA28 complexes, which also contain PA700 (8). The PA28 family comprises three members: α, β, and γ. PA28α encoded by the *PSME1* gene and PA28β encoded by the *PSME2* gene form a heteropolymer, which is mainly located in the cytoplasm, whereas PA28γ encoded by the *PSME3* gene forms a homopolymer that predominantly occurs in the nucleus (9). The association of the PA28 with the 20S may play a role in antigen processing by modulating peptide cleavage in the 20S (10,11), but it appears that the PA28 may play a greater role in intracellular protein degradation than in antigen processing (12). Recently, it was reported that PA28α overexpression enhances ubiquitin-proteasome system–mediated degradation of abnormal proteins (13).

It has been reported that fatty acids, insulin (14), and oxidative stress (15) inhibit proteasome activity in cultured hepatocellular carcinoma (Hep)G2 cells. However, it remains to be determined whether liver proteasome function is dysregulated in obesity and type 2 diabetes.

Based on these findings, we hypothesized that proteasome dysregulation in the liver is involved in the development of hepatic insulin resistance in obesity and type 2 diabetes. To test this hypothesis, we generated PA28α-PA28β-PA28γ triple-knockout (PA28 KO) mice as a model of impaired proteasome function and investigated their metabolic phenotypes.

RESEARCH DESIGN AND METHODS

Human studies. This study was approved by the ethics committee of Kanazawa University. Liver biopsy specimens were obtained from 21 patients with type 2 diabetes (15 men and 6 women; mean age 53.0 ± 2.1 years, BMI 24.4 ± 0.9 kg/m^2, fasting plasma glucose 7.94 ± 0.59 mmol/L, HbA_{1c} 7.3 ± 0.3%, and alanine aminotransferase 34.4 ± 5.5 IU/L) admitted to Kanazawa University Hospital between 2000 and 2003 as previously described (5,16). Statistical analyses of DNA chip gene expression data were performed as previously

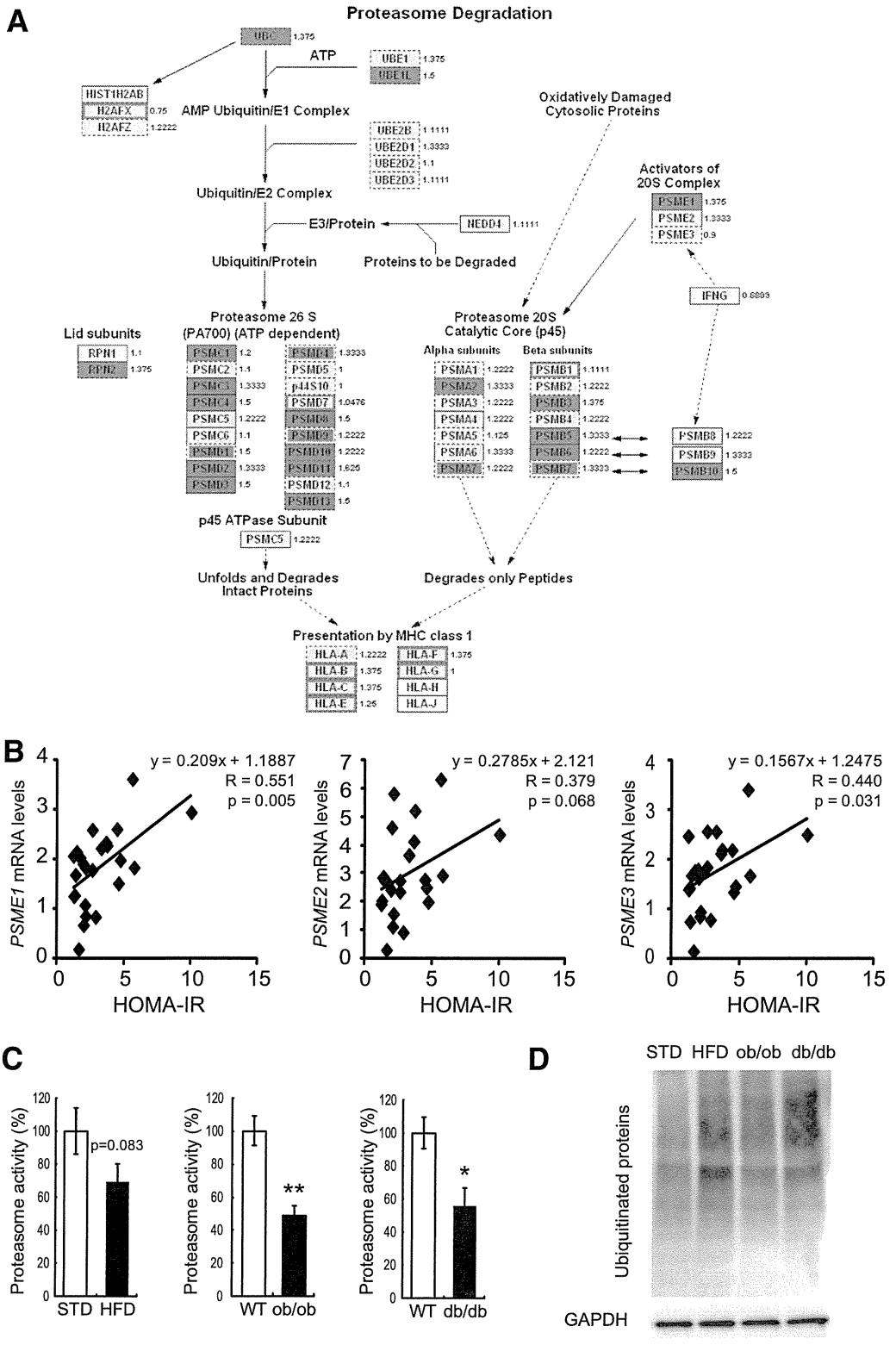

FIG. 1. Proteasome dysfunction in mouse models of obesity. ***A*****: Gene expression and proteasome activity in the livers of patients with type 2 diabetes and obesity. Coordinate upregulation of genes involved in proteasome degradation pathways in the livers of type 2 diabetic patients with obesity compared with those without obesity. GenMAPP (Gene MicroArray Pathway Profiler [http://www.genmapp.org]) was used to annotate the pathway with expression ratios for the genes involved. The fold changes presented beside the gene names are for obese versus nonobese patients. Genes significantly upregulated in obesity ($P < 0.05$) are shown in red; genes analyzed whose expression was not significantly altered in obesity are shown in gray.** ***B:*** **Graphs showing associations between homeostasis model assessment of insulin resistance (HOMA-IR) and the mRNA expression of subunits of PA28: PA28α (*PSME1*), PA28β (*PSME2*), and PA28γ (*PSME3*). Data were normalized according to 18S mRNA level.** ***C*****: Comparison of liver proteasome activity in 32-week-old C57BL6 mice fed STD and HFD for 28 weeks (from 4 to 32 weeks of age), in WT and *db/db* mice (20 weeks old), and in WT mice and *ob/ob mice* (20 weeks old). Proteasome activity was estimated by measuring chymotrypsin-like activity**

described (5). To test the significance of expression ratios for individual genes or pathways, we performed a supervised analysis using a permutation-based method with BRB-ArrayTools software (17), developed for the statistical analysis of DNA chip gene expression data by the Biometric Research Branch of the U.S. National Cancer Institute.

Animal experiments. PA28 KO mice were generated by cross-breeding PA28α-PA28β double-KO mice (18) and PA28γ KO mice (19). Genetic background of both lines of KO mice is almost completely homologous to that of C57BL/6J mice because they were backcrossed to C57BL/6J mice for at least eight generations. C57BL/6J mice and *ob/ob* mice were obtained from Sankyo Laboratory Service (Tokyo, Japan), and genetically diabetic model male *db/db* mice were obtained from Charles River (Tokyo, Japan). The study protocol was reviewed and approved by the animal care and use committee of Kanazawa University. All mice were housed in specific pathogen-free barrier facilities, maintained under a 12-h light/dark cycle, fed a standard rodent food diet (Oriental Yeast) (STD) or rodent food containing 60% fat (Research Diet) (HFD) for up to 28 weeks, and provided with water ad libitum. Sodium 4-phenylbutyrate (PBA, Enzo Life Sciences, Farmingdale, NY) was mixed in drinking water at a concentration of 4 mg/mL and administered ad libitum for 3 weeks as previously described (20).

Gene expression analyses in mice. We used Genopal DNA chips (21) (Mitsubishi Rayon, Tokyo, Japan [http://www.mrc.co.jp/genome/e/index.html]) and RT-PCR to identify significant changes in hepatic gene transcription. Total RNA was isolated using an RNeasy Mini Kit (Qiagen, Valencia, CA) and converted into cDNA using a cDNA synthesis kit (Applied Biosystems, Tokyo, Japan) as previously described (22). Quantitative real-time PCR analysis was performed on an ABI Prism 7900HT Sequence Detection System (Invitrogen) using TaqMan gene expression assays (Applied Biosystems) or the SYBR Green Master Mix (Takara Bio, Otsu, Japan) as described previously (23). The primers for mouse acetyl-CoA carboxylase-1 (*Acc1*) were as follows: forward, 5′-TGGAGAGCC CCACACACA-3′; reverse, 5′-TGACAGACTGATCGCAGAGAAAG-3′. The primers for mouse X box-binding protein 1 (XBP-1) were as follows: forward, 5′-AAACAGAGTAGCAG-CGCAGACTGC-3′; reverse, 5′-GGATCTCTAAAACTAGAGGCTTGGTG-3′. The primers for mouse C/EBP homologous protein (CHOP) were as follows: forward, 5′-TATCTCATCCCCAGGAAACG-3′; reverse, 5′-GGGCACTGACCACTCTGTTT-3′. TaqMan gene expression assays (Applied Biosystems) were used for *PSME1* (Hs00389209_m1); *PSME2* (Hs01581609_g1); *PSME3* (Hs00195072_m1); *Psme1* (Mm00650858_g1); *Psme2* (Mm01702832_g1); *Psme3* (Mm00839833_m1); insulin receptor substrate 2 (Irs2) (Mm03038438_m1); sterol regulatory element–binding factor 1 (*Srebf1*) (Mm00550338_m1); forkhead box O1 (*Foxo1*) (Mm00490672_m1); glucose-6-phosphatase, catalytic (*G6pc*) (Mm00839363_m1); phosphoenolpyruvate carboxykinase 1 (*Pck1*) (Mm01247058_m1); insulin-like growth factor binding protein 1 (*Igfbp1*) (Mm00515154_m1); and peroxisome proliferator–activated receptor γ coactivator 1α (*Ppargc1a*) (Mm01208835_m1).

Determination of proteasome activity. Frozen livers were minced and homogenized in ice-cold buffer (25 mmol/L Tris-HCl [pH 7.5], containing 1 mmol/L dithiothreitol and 2 mmol/L ATP) using an homogenizer and then frozen and thawed three times. Extracts were centrifuged at 12,000 rpm for 10 min at 4–8°C. Protein concentrations were determined using the Lowry Protein Assay (Bio-Rad Laboratories, Richmond, CA). Proteasome activity was assayed as chymotrypsin-like activity in proteasome assay buffer containing 100 mmol/L Tris-HCl (pH 8.0), 2 mmol/L ATP, and fluorogenic peptide substrate (0.1 mmol/L) according to a procedure previously described (24). The assay for chymotrypsin-like activity is based on the detection of the fluorophore 7-amino-4-methylcoumarin (AMC) after its cleavage from the labeled substrate Suc-Leu-Leu-Val-Tyr-AMC (Peptide Institute, Osaka, Japan). Free AMC fluorescence was quantified using a 355/460 nm filter set in a luminescence spectrophotometer (Fluoroskan Ascent FL; ThermoLab Systems, Franklin, MA). Proteasome activity was calculated as the difference between the total activity in tissue extracts and the remaining activity in the presence of the proteasome inhibitor MG132 (20 μmol/L).

Immunoprecipitation and Western blotting. Proteins were extracted from tissues and subjected to SDS-PAGE as previously described (25). Membranes were incubated overnight at 4°C with antibodies against ubiquitin (DAKO Japan, Kyoto, Japan), PA28α (Cell Signaling Technology, Danvers, MA), PA28β (Cell Signaling Technology), PA28γ (Cell Signaling Technology), Akt (Cell Signaling Technology), phosphorylated (p)–Ser473-Akt (p-Akt) (Cell Signaling), IRS-1 (Millipore, Billerica, MA), p–IRS-1 (Ser307) (Cell Signaling Technology), IRS-2 (Cell Signaling Technology), phosphatidylinositol 3-kinase p85 (PI3K p85; Millipore Corp.), SREBP-1 (Santa Cruz Biotechnology, Santa Cruz, CA), pan-cadherin (Cell Signaling), glucose-regulated protein 78 (GRP78) (Santa Cruz Biotechnology), immunoglobulin heavy-chain binding protein (BiP) (Cell Signaling), p–protein kinase R–like endoplasmic reticulum kinase (p-PERK) (Cell Signaling), inositol-requiring enzyme (IRE) 1α (Novus Biologicals, Littleton, CO), p-IRE1α (Novus), eukaryotic initiation factor 2α (eIF2α) (Cell Signaling), p-eIF2α (Cell Signaling), XBP-1 (Santa Cruz Biotechnology), c-Jun NH_2-terminal kinase (JNK) (Cell Signaling), p-JNK (Cell Signaling), p–c-Jun (Santa Cruz Biotechnology), and CHOP (Cell Signaling). The membranes were incubated with secondary antibody conjugated with enhanced chemiluminescence Western Blotting Detection Reagents (GE Healthcare) and were visualized using an LAS-3000 luminescent image analyzer (FUJIFILM, Tokyo, Japan). Glyceraldehyde-3-phosphate dehydrogenase (GAPDH) (Santa Cruz Biotechnology) was used as a control for protein loading.

Measurement of biochemical parameters. Plasma glucose levels, blood insulin levels, and triglyceride content in the liver were determined with a Glucocard Diameter, (ARKRAY, Kyoto City, Japan), an insulin kit (Morinaga, Yokohama, Japan), and TG-E Test Wako kits (Wako, Osaka, Japan), respectively.

Glucose and insulin tolerance tests and insulin infusion. Glucose and insulin tolerance tests were performed through injection of glucose (1–1.5 g/kg i.p.) and insulin (2.0 IU/kg i.p.), respectively, after an overnight fast. After the withdrawal of food for 4 h, mice were anesthetized. Twenty minutes after an injection of insulin (10 IU/kg i.p.), tissues were removed, frozen in liquid nitrogen, and stored at −80°C until processing.

Hyperinsulinemic-euglycemic clamp studies in mice. Clamp studies were performed after 2–3 days of recovering from cannulization as previously described (25). Clamp studies were performed on conscious and unrestrained animals. During clamp studies, insulin (Novolin R; Novo Nordisk, Denmark) was continuously infused at a rate of 5.0 mU/kg/min, and the blood glucose concentration (monitored every 5 min) was maintained at 100 mg/dL through the administration of glucose (50% enriched to ~20% with [6,6-$^2H_2$]glucose; Sigma) for 120 min. Blood was sampled through tail-tip bleeds at 90, 105, and 120 min for the purpose of determining the glucose R_d. R_d values were calculated according to non–steady-state equations, and hepatic glucose production was calculated as the difference between the R_d and the exogenous glucose infusion rates.

Histopathological examination. Liver samples were fixed in 4% buffered formalin and embedded in Tissue-Tek OCT compound (Sakura Finetek USA) and paraffin for histological analysis. The formalin-fixed and paraffin-embedded section (5 mm) was processed routinely for hematoxylin-eosin staining. The OCT-embedded samples were serially sectioned at 4 mm. For the evaluation of fat deposition, the liver section was stained with Oil-red O.

Preparation for nuclear matrix and cell membrane fractions from whole cell lysates. Nuclear matrix and cell membrane fractions were extracted from whole cell lysates by using the CNMCS compartmental protein extraction kit (BioChain Institute) according to the manufacturer's protocol.

Electron microscopy. Small pieces of mouse liver were fixed through incubation with 2% paraformaldehyde and 2% glutaraldehyde in 0.1 mol/L phosphate buffer (pH 7.2) for 2 h at 4°C and then postfixed through incubation with 1% OsO_4 for 2 h at 4°C. Specimens were stained with 1% uranium acetate for 30 min, dehydrated in a graded ethanol series, and embedded in an epoxy resin based on Glycidether (Selva Feinbiochemica, Heidelberg, Germany). Ultrathin sections were prepared using an ultramicrotome, stained with uranium acetate and lead citrate, and visualized using a JEM-1210 electron microscope (JEOL, Tokyo, Japan).

Cell culture. Studies were performed using H4IIEC3 rat hepatoma cells that were purchased from the American Type Culture Collection (Manassas, VA). Cells were maintained in Dulbecco's modified Eagle's medium (DMEM) (Invitrogen) supplemented with 10% FBS (Invitrogen), penicillin (100 units/mL), and streptomycin (0.1 mg/mL; Invitrogen) at 37°C under an atmosphere of 5% CO_2 in air in a humidified incubator.

Chemicals. Bortezomib was purchased from LC laboratories (Woburn, MA). PBA for in vitro experiments was purchased from Calbiochem (San Diego, CA).

Statistical analysis. All data are expressed as means ± SE and were analyzed by the Mann-Whitney *U* test with the level of statistical significance set at $P < 0.05$. All calculations were performed using SPSS, version 11.0, software for Windows (SPSS, Chicago, IL).

RESULTS

Expression of genes involved in proteasome pathways is altered in the livers of patients with type 2 diabetes and obesity. We previously identified metabolic pathways that are altered in association with obesity in the livers of

in liver tissues as described in RESEARCH DESIGN AND METHODS. Data represent means ± SE (n = 4 per group). *$P < 0.05$, **$P < 0.01$. *D*: Accumulation of polyubiquitinated proteins was assessed by Western blot in the livers isolated from C57BL6 mice fed the STD and the HFD, *db/db* mice, and *ob/ob* mice. GAPDH served as internal control.

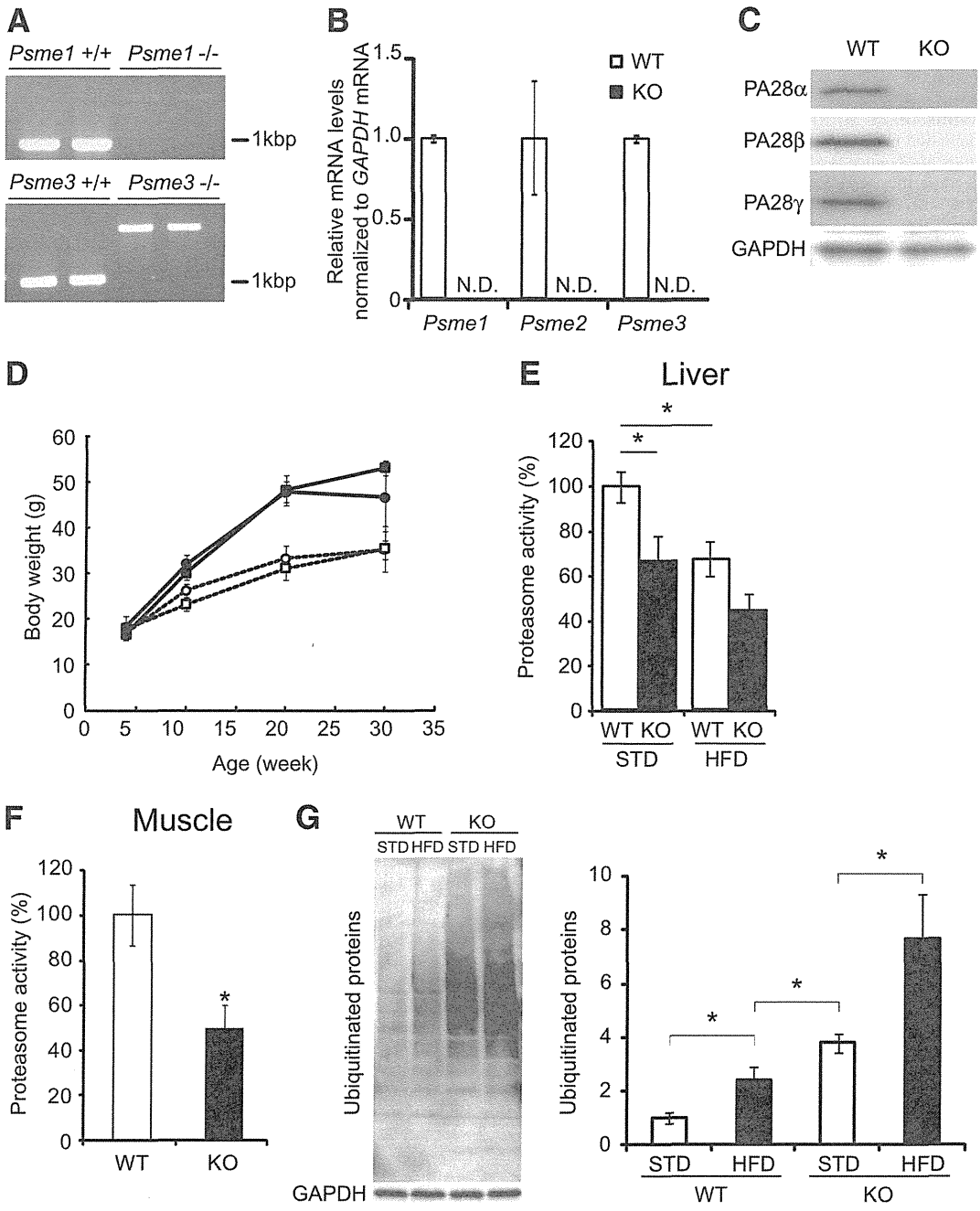

FIG. 2. PA28 KO mice show impaired proteasome function and accumulation of polyubiquitinated proteins in the liver. *A*: Mice were genotyped by PCR analysis as previously described (18,19). Genomic DNA extracted from mouse tails was analyzed by PCR. Primers used for genotyping were 5'-TTTCCTGTACGTGACTTCCATCCTGTTG-3' (primer 1), 5'-GGTCCACATACAATAAAGACATGGGCTG-3' (primer 2), and 5'-GATTGTGGTCCTCCT GCAACGCCTAAA-3' (primer 3). Primers 1 and 3 amplified 1.2-kb fragments from the wild-type PA28α allele. Primers 1 and 2 amplified 2.2-kb fragments from the mutant allele. Primers used for genotyping were 5'-CCGGGACAATAAGACACATCACTC-3' (primer 1), 5'-TTGTCCCTCC CTCCAGTTGTCTAA-3' (primer 2), and 5'-GATCCCCTCAGAAGAACTCGTCAA-3' (primer 3). Primers 2 and 3 amplified 0.9-kb fragments from the wild-type PA28γ allele. Primers 1 and 3 amplified 1.9-kb fragments from the mutant allele. *B*: RT-PCR analysis of total RNA prepared from liver of PA28 KO mice (n = 7). N.D., not determined. Transcripts of mouse PA28α, -β, and -γ were examined by quantitative RT-PCR. Data were normalized according to *GAPDH* mRNA level and presented as a value relative to that for WT mice. *C*: Western blot analysis of extracts prepared from the liver of PA28 KO mice. The blot was probed with the anti-PA28α, anti-PA28β, and anti-PA28γ antibodies. *D*: Body weights of WT and PA28 KO mice fed an STD or the HFD. ○, WT mice fed the STD (n = 5); ●, WT mice fed the HFD (n = 4); □, PA28 KO mice fed the STD (n = 4); ■, PA28 KO mice fed the HFD (n = 4). Data represent means ± SE. *E*: Comparison of liver proteasome activity in WT (n = 13, STD; n = 4, HFD) and PA28 KO (n = 11, STD; n = 4, HFD) mice. Data represent means ± SE. *$P < 0.05$. *F*: Proteasome activity was evaluated in the muscles isolated from 32-week-old WT mice (n = 5) and PA28 KO mice (n = 4). The activity was normalized to the total protein content. Data represent means ± SE. *$P < 0.05$. *G*: Western blot analyses of total ubiquitinated proteins in the livers of WT and KO mice. Livers were isolated from 32-week-old WT and PA28 KO mice fed the STD or the HFD for 28 weeks (from 4 to 32 weeks of age). Quantitation of ubiquitinated proteins levels is normalized to GAPDH and is represented as means ± SE (n = 3 per group). *$P < 0.05$.

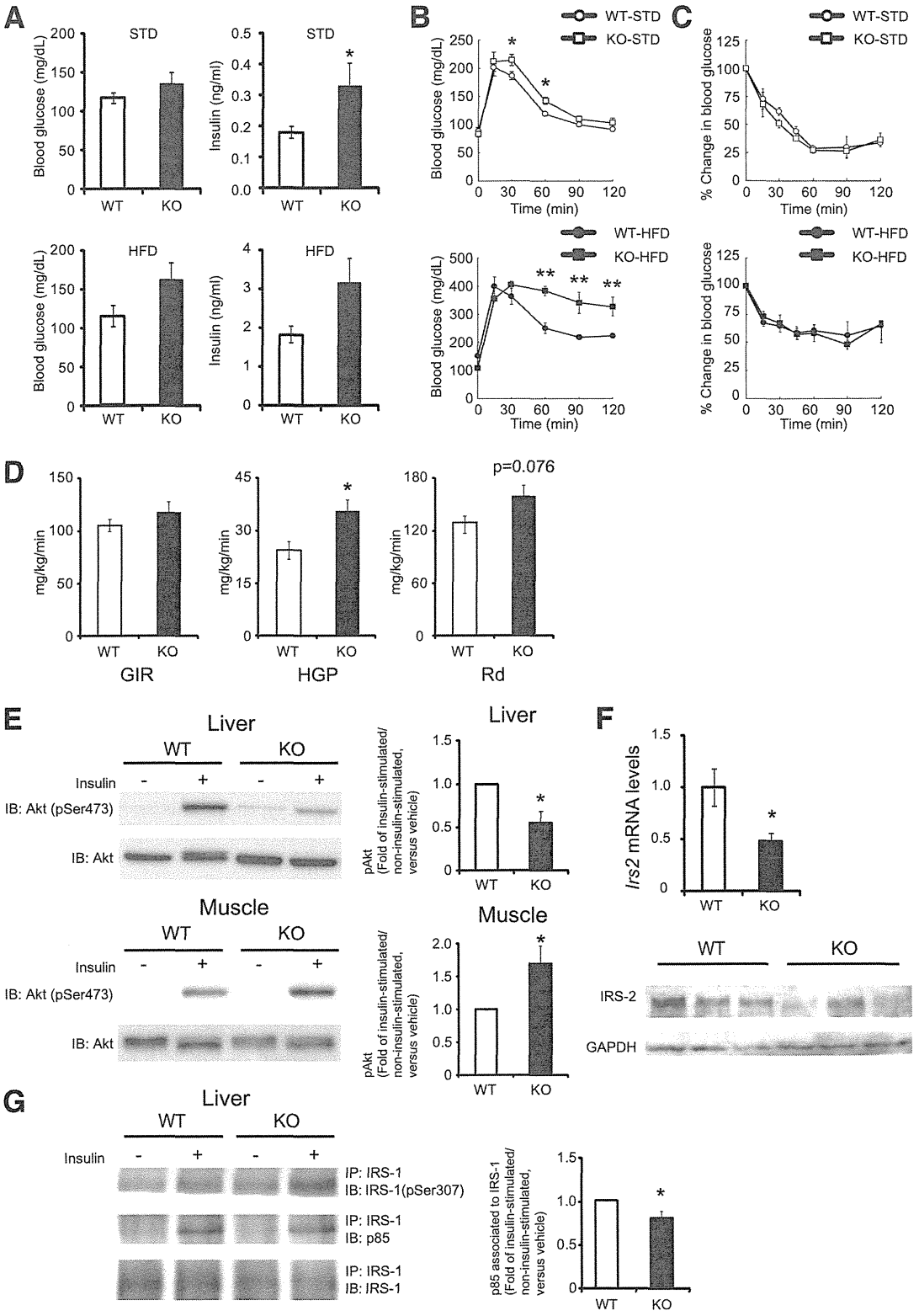

FIG. 3. PA28 KO mice show proteasome dysfunction, glucose intolerance, and attenuated insulin signaling in the liver. ***A*****: Blood glucose concentrations and serum insulin levels measured in an overnight fasting state at 20 weeks of age. WT (n = 9, STD; n = 5, HFD) and PA28 KO (n = 6, STD; n = 4, HFD) mice. Data represent means ± SE. *P < 0.05.** ***B*****: Intraperitoneal glucose tolerance tests (IPGTT).** ***C*****: Intraperitoneal insulin tolerance tests (IPITT). Blood glucose level measured during the intraperitoneal glucose tolerance tests and intraperitoneal insulin tolerance tests at 20 weeks of age. WT mice fed the STD, n = 5; WT mice fed the HFD, n = 4; PA28 KO mice fed the STD, n = 4; PA28 KO mice fed the HFD, n = 4. Data represent means ± SE. *P < 0.05. **P < 0.01.** ***D*****: Insulin sensitivity was assayed by using a hyperinsulinemic-euglycemic clamp study in WT (n = 8) and PA28 KO (n = 10) mice.** ***Left panel*****: Glucose infusion ratio.** ***Middle panel*****: HGP before and after insulin clamp.** ***Right panel*****: Glucose disposal rate. Data represent means ± SE. *P < 0.05.** ***E*****: Equal amounts of protein in total lysates of liver and muscle were immunoblotted (IB) with anti–p-Akt (Ser473) and anti-Akt antibodies. p-Akt values of insulin-injected fasted mice were displayed relative to those of saline-injected**

patients with type 2 diabetes (5,16). Clinical characteristics of study obese and nonobese subjects are shown in Supplementary Table 1. The hepatic expression of genes involved in a proteasome pathway, the gene encoding PA28α ($P < 0.05$), was coordinately upregulated in diabetic patients who were obese compared with those who were not obese (Fig. 1*A*). To further strengthen the significance of the hepatic expression of the genes for PA28s, we analyzed an independent new sample set of the human liver using RT-PCR. Clinical information of the subjects is described in Supplementary Table 2. As shown in Fig. 1*B*, mRNA levels of genes encoding PA28α, -β, and -γ in the human liver correlated positively with an insulin resistance index (homeostasis model assessment of insulin resistance). Therefore, hepatic expression of PA28s was associated with insulin resistance in humans. We next analyzed hepatic gene expression in a mouse model of diet-induced obesity (HFD mice) using a custom-made array, Metabolic Chip (21). Consistent with human data, the hepatic expression of genes involved in the proteasome pathway was coordinately upregulated in C57BL/6 mice fed the HFD compared with those fed the STD. Of these, the gene encoding PA28β (*Psme2*) was significantly upregulated in mice fed the HFD compared with those fed the STD (Supplementary Table 3). These findings prompted us to test the hypothesis that proteasome degradation pathways are involved in the development of obesity-induced insulin resistance in the liver.

Liver proteasome activity is reduced in animal models of type 2 diabetes and obesity. Next, we examined liver proteasome activity in animal models of type 2 diabetes and obesity. Proteasome activity was measured using a substrate for chymotrypsin-like activity. Unexpectedly, liver proteasome activity was reduced by ~30–40% in genetically obese *ob/ob* mice, diabetic *db/db* mice, and C57BL/6 mice fed the HFD (Fig. 1*C*). As a consequence, accumulation of ubiquitinated proteins was increased in the liver of C57BL/6 mice fed the HFD, *db/db* mice, and *ob/ob* mice (Fig. 1*D*). These results suggest that liver proteasome activity is reduced in animal models of type 2 diabetes and obesity. Coordinate upregulation of genes involved in the ubiquitin-proteasome pathway in obese patients and mouse models of type 2 diabetes and obesity may compensate for impaired proteasome function.

PA28 KO mice show impaired proteasome function and accumulation of polyubiquitinated proteins in the liver. To test the hypothesis that proteasome dysregulation in the liver is involved in the development of hepatic insulin resistance in obesity and type 2 diabetes, we generated a mouse model of impaired proteasome function: PA28 KO mice. We first performed a genomic DNA PCR analysis to confirm that the mutant mice expressed the messages of neither the PA28α nor the PA28γ gene (Fig. 2*A*). Knockout of the *Psme1*, *Psme2*, and *Psme3* in the liver of PA28 KO mice was confirmed both by RT-PCR and by Western blotting analyses (Fig. 2*B* and *C*). Up to 30 weeks after birth, PA28 KO mice were indistinguishable in appearance and growth from age-matched wild-type (WT) mice (Fig. 2*D*).

When fed the STD, PA28 KO mice had 35% reduced hepatic proteasome activity compared with WT mice (Fig. 2*E*). Proteasome activity was also reduced by ~50% in the skeletal muscle of PA28 KO mice compared with that of WT mice (Fig. 2*F*). These results are consistent with previous observations in mouse embryonic fibroblasts from $PA28\alpha^{-/-}PA28\beta^{-/-}$ mice (18). The degree of proteasome inactivation in the livers of PA28 KO mice corresponded with that in the livers of *db/db* mice and C57BL mice fed the HFD (Fig. 1*C* and Fig. 2*E*). Thus, the PA28 KO mouse appears to be an appropriate animal model that mimics the proteasome dysfunction observed in obesity and type 2 diabetes. When fed the HFD, PA28 KO mice tended to have further reduced hepatic proteasome activity compared with WT mice ($P = 0.086$) (Fig. 2*E*).

For assessment of the impact of proteasome dysfunction in the liver, polyubiquitinated proteins were detected by Western blotting (Fig. 2*G*). The HFD increased the accumulation of ubiquitinated proteins in the liver in both WT and PA28 KO mice. As expected, more polyubiquitinated proteins accumulated in the livers of PA28 KO mice compared with those of WT mice for both STD-fed and HFD-fed mice. Accumulation of the ubiquitinated proteins in the liver of PA28 KO mice fed HFD was significantly increased compared with those fed STD, suggesting that HFD further impairs proteasome function in PA28 KO mice.

PA28 KO mice show glucose intolerance and attenuated insulin signaling in the liver. To examine the metabolic effects of proteasome dysfunction in vivo, we performed glucose and insulin loading tests. Fasting glucose levels were similar in PA28 KO mice and WT mice (Fig. 3*A*). However, PA28 KO mice showed glucose intolerance after glucose loading (Fig. 3*B*), which was further exacerbated by the HFD (Fig. 3*B*). While serum insulin levels were significantly higher in PA28 KO mice compared with WT mice (Fig. 3*A*), there was no significant difference in insulin tolerance test results (Fig. 3*C*), suggesting the existence of hepatic insulin resistance in the PA28 KO mice.

Because the PA28 KO mouse appears to be a model that mimics the proteasome dysfunction observed in HFD-fed mice, subsequent experiments were performed only in mice fed the STD. To identify the responsible organ that contributes to insulin resistance in PA28 KO mice, we next performed hyperinsulinemic-euglycemic clamp experiments and Western blot analysis of the insulin-signaling pathway. As shown in Fig. 3*D*, endogenous glucose production was significantly increased in PA28 KO mice, whereas peripheral glucose disposal tended to be increased. In the liver of PA28 KO mice, insulin-induced phosphorylation of Akt at Ser473 was impaired (Fig. 3*E*) in association with marked reduction in IRS-2 protein levels (Fig. 3*F*) and enhanced serine phosphorylation of IRS-1 compared with WT mice (Fig. 3*G*). Insulin-induced increment in IRS-1–associated p85 subunit of PI3K was slightly impaired in the liver of PA28 KO mice compared with that of WT mice (Fig. 3*G*). On the other hand, in the skeletal muscle of the PA28 KO mice, insulin-induced phosphorylation of Akt at Ser473 was rather enhanced

mice (WT mice fed the STD, $n = 7$; PA28 KO mice fed the STD, $n = 7$). Data represent means ± SE. *$P < 0.05$. *F*: Expression of mRNAs encoding *Irs2* in the livers of 12-week-old WT and PA28 KO mice analyzed by quantitative real-time RT-PCR. Expression values were normalized to *18S* mRNA. Data represent means ± SE ($n = 7$ per group). *$P < 0.05$. Liver lysates from mice were immunoblotted with anti–IRS-2 antibody. *G*: Liver lysates from mice were immunoprecipitated (IP) using anti–IRS-1 antibody bound to protein A agarose. The immunoprecipitates were immunoblotted with anti–p–IRS-1 (Ser307) and p85. Representative results from five mice of each genotype are shown. *Right panel*: densitometry quantitation of IRS-1 to p85 signal ratio is shown. Data represent means ± SE. *$P < 0.05$.

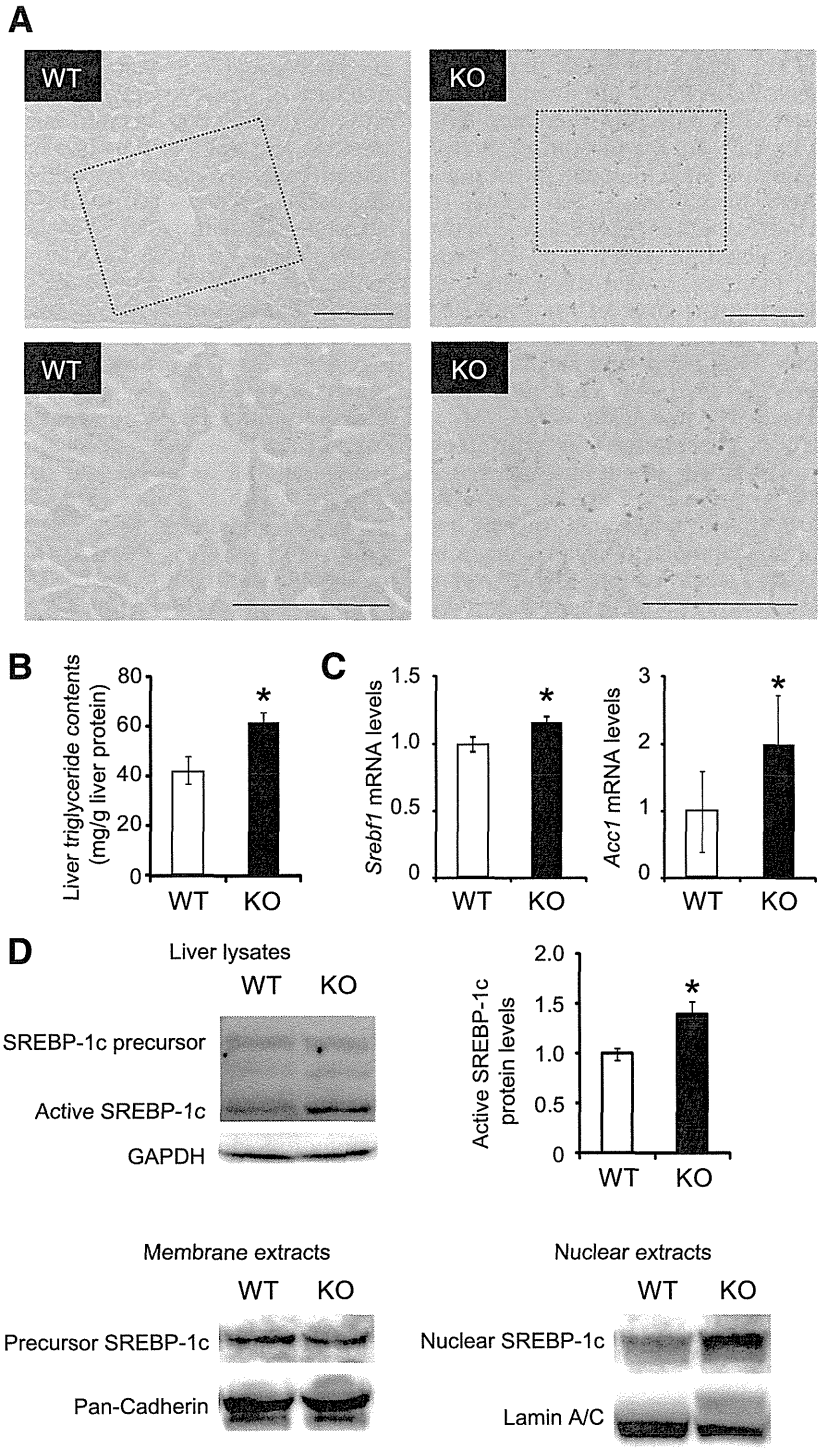

FIG. 4. PA28 KO mice show hepatic SREBP-1c activation and steatosis. *A*: Oil-red O staining of lipid droplets in the livers of 12-week-old WT and PA28 KO mice. The highlighted region of the *upper panel* is shown at a higher magnification in the *lower panel*. Scale bars, 100 μm. *B*: Triglyceride contents in the livers of WT and PA28 KO mice. Data are expressed as milligrams per gram of liver tissue. Data represent means ± SE (n = 4–5 per group). *P < 0.05. *C*: Expression of mRNAs encoding *Srebf1* and *Acc1* in the livers of 12-week-old WT and PA28 KO mice analyzed by quantitative real-time RT-PCR. Expression values were normalized to *GAPDH* mRNA. Data represent means ± SE (n = 7–9 per group). *D*: Whole cell, membrane, and nuclear fractions in liver extracts were subjected to SDS-PAGE and blotted using an anti–SREBP-1 antibody. GAPDH, pan-cadherin, and lamin A/C served as internal controls. Quantitation of SREBP-1 68-kDa protein levels is normalized to GAPDH and is represented as means ± SE. *P < 0.05.

compared with that of WT mice (Fig. 3*E*). These findings indicate that PA28 deficiency impairs insulin signaling mainly in the liver and thereby induces systemic glucose intolerance in vivo.

PA28 KO mice show hepatic steatosis. In insulin-resistant states, the hyperinsulinemia drives hepatic lipogenesis via a SREBP-1c pathway (26). Oil-red O staining of liver tissue sections revealed a slight hepatic steatosis in

the PA28 KO mice fed STD (Fig. 4*A*). Triglyceride content was significantly increased in the liver of PA28 KO mice (Fig. 4*B*). To understand the molecular basis underlying the enhanced hepatic steatosis in PA28-null livers, we analyzed gene expression of SREBP-1c that regulates lipid biosynthesis. As shown in Fig. 4*C*, expression of *Srebf1* was modestly increased in the PA28-deleted livers compared with control livers. Furthermore, the levels of cleaved/active SREBP1c were much more increased in the liver of the PA28 KO mice compared with that of WT mice (Fig. 4*D*). Indeed, mRNA expression of *Acc1*, a target of SREBP-1c, was upregulated in the liver of the PA28 KO mice compared with that of WT mice (Fig. 4*C*). Nuclear SREBP-1c, but not membrane-bound precursor of SREBP-1c, was significantly increased in the livers of PA28 KO mice compared with those of WT mice (Fig. 4*D*).

PA28 deficiency–induced proteasome dysfunction activates an unfolded protein response and increases ER stress in the liver. To investigate the mechanisms underlying proteasome dysfunction–induced insulin resistance in the liver, we evaluated morphological changes in the liver through histological examination. Hematoxylin-eosin staining of liver tissues showed that hepatocytes were indistinguishable in the two groups (Fig. 5*A*). Next, we examined morphological changes in organelles within hepatocytes by electron microscopy. Electron micrographs revealed massive expansion of the ER in the livers of PA28 KO mice (Fig. 5*B*), suggestive of an unfolded protein response (UPR) (27). ER stress is caused by the accumulation of unfolded and misfolded proteins in the ER lumen and is associated with several human diseases (28,29). In addition, proteasome inhibitors have been reported to induce ER stress in cultured primary rat hepatocytes (30). Therefore, to examine whether PA28 deficiency–induced proteasome dysfunction causes ER stress in the liver, we analyzed the expression patterns of several molecular indicators of ER stress in liver extracts from 12-week-old WT and PA28 KO mice fed the STD (Fig. 5*C* and *D*). Proteasome dysfunction induced by PA28 gene deletion resulted in ER stress in the liver tissues of lean mice, as evidenced by increased levels of Grp78, CHOP, p-PERK, p-eIF2α, and p-IRE1α, as well as ER stress–inducible mRNAs encoding CHOP and the spliced form of XBP-1 (XBP-1s), compared with WT mice (Fig. 5*C* and *D*). XBP-1s protein amounts in nuclear fractions increased significantly in the liver tissue of PA28 KO mice compared with that of WT mice (Fig. 5*C*). Hyperactivation of JNK through phosphorylation is another marker of ER stress (31) and plays a role in linking ER stress and insulin resistance (32). Phosphorylation of JNK and its downstream target c-Jun was significantly increased in the livers of PA28 KO mice compared with those of WT mice (Fig. 5). Based on these findings, it might be possible that general accumulation of polyubiquitinated proteins or accumulation of some specific substrate for PA28s promotes a UPR and ER stress in the livers of PA28 KO mice.

Proteasome dysfunction–induced ER stress and insulin resistance are partly blocked by an orally active chemical chaperone, PBA, in the liver of PA28 KO mice. We next investigated the effects of PBA administration on proteasome dysfunction–induced ER stress and insulin resistance in PA28 KO mice. Intraperitoneal glucose tolerance test was performed to further evaluate the effect of PBA on whole-body glucose metabolism. After glucose loading, blood glucose levels tended to decrease in PBA-administered PA28 KO mice compared with untreated PA28 KO mice (Supplementary Fig. 1). The plasma insulin levels after glucose loading significantly increased in PBA-administered PA28 KO mice compared with untreated PA28 KO mice (Supplementary Fig. 1). Administration of PBA ameliorated massive expansion of the ER in the livers of PA28 KO mice (Fig. 6*A*) and decreased hepatic CHOP expression and IRE1a phosphorylation, suggesting that PBA administration alleviates hepatic ER stress in PA28 KO mice (Fig. 6*B*). As a consequence, PBA administration improved impaired insulin-induced phosphorylation of Akt at Ser473 in liver tissue of PA28 KO mice (Fig. 6*C*). These findings confirm the critical role of ER stress in the proteasome dysfunction–mediated insulin resistance.

PA28 deficiency–induced proteasome dysfunction increases FoxO1 protein amounts and gluconeogenic genes in the liver. It has been shown that the FoxO1 protein is targeted for proteasomal degradation (33–35). FoxO1 protein amounts dramatically increased in total cell lysates as well as in nuclear fractions of PA28 KO mice compared with WT mice (Fig. 7*A*), whereas *Foxo1* mRNA levels were unaltered (Fig. 7*B*). In addition, FoxO1 phosphorylation was decreased in the liver tissue of PA28 KO mice compared with that of WT mice (Fig. 7*A*). Gluconeogenic genes, such as *Pck1* and *Igfbp1*, which are targets of FoxO1 were upregulated in the livers of PA28 KO mice compared with those of WT mice (Fig. 7*C*). These findings suggest that impaired degradation of FoxO1 is one of the candidate pathways leading to impaired suppression of gluconeogenic genes and increased hepatic glucose production in PA28 KO mice.

Proteasome inhibition causes ER stress and insulin resistance in vitro—responses that are partly blocked by a chemical chaperone. To confirm that proteasome dysfunction causes ER stress and insulin resistance at the cellular level, we pretreated rat hepatoma-derived H4IIEC3 cells with bortezomib, a selective inhibitor of the 26S proteasome. Bortezomib concentration-dependently increased levels of UPR molecular markers, such as BiP, CHOP, and phosphorylated forms of IRE1α and JNK (Fig. 8*A*). Bortezomib also reduced insulin-stimulated serine phosphorylation of Akt at Ser473 in H4IIEC3 hepatocytes in a concentration-dependent manner (Fig. 8*B*). To address whether ER stress is responsible for proteasome dysfunction–induced insulin resistance, we tested the effect of the chemical chaperone PBA on H4IIEC3 cells treated with bortezomib. PBA partly prevented the accumulation of BiP and CHOP, the phosphorylation of JNK (Fig. 8*C*), and the impaired phosphorylation of Akt at Ser473 (Fig. 8*D*) induced by bortezomib. These findings indicate that proteasome dysfunction at least partly accelerates insulin resistance via ER stress in hepatocytes.

DISCUSSION

Our study shows that liver proteasome activity is reduced by ~30–40% in genetic and dietary models of obesity and diabetes with coordinate upregulation of genes involved in the ubiquitin-proteasome pathway. In concert with our findings, recent systematic analyses of liver tissue in obese mice also revealed increased proteasome components (36,37), which may compensate for impaired proteasome function. To test a hypothesis that proteasome dysfunction may be a primary event that links obesity and insulin resistance in the liver, we established a mouse model of impaired proteasome function by deleting PA28 genes. The livers of PA28 KO mice showed impaired proteasome function similar to that observed in mouse models of